THESIS

PERFORMANCE EVALUATION OF MULTIPLE OXIDATION CATALYSTS ON A LEAN BURN NATURAL GAS ENGINE

Submitted by

Koushik Badrinarayanan

Department of Mechanical Engineering

In partial fulfillment of the requirements

For the Degree of Master of Science

Colorado State University

Fort Collins, Colorado

Spring 2012

Master's Committee:

Advisor: Daniel B. Olsen

Anthony Marchese
Michael A. De Miranda

ABSTRACT

PERFORMANCE EVALUATION OF MULTIPLE OXIDATION CATALYSTS ON A LEAN BURN NATURAL GAS ENGINE

Emission from lean burn natural gas engines used for power generation and gas compression are major contributors to air pollution. Two-way catalysts or oxidation catalysts are the common after-treatment systems used on lean burn natural gas engines to reduce CO, VOCs and formaldehyde emissions. The performance of the oxidation catalysts is dependent on operating parameters like catalyst temperature and space velocity. For this study, a part of the exhaust from a Waukesha VGF-18 GL lean burn natural gas engine was flowed through a catalyst slipstream system to access the performance of the oxidation catalysts. The slipstream is used to reduce the size of the catalysts and to allow precise control of temperature and space velocity. Analyzers used include Rosemount 5-gas emissions bench, Nicolet Fourier Transform Infra-Red spectrometer and HP 5890 Series II Gas Chromatograph. The oxidation catalysts were degreened at 1200^{o}F (650^{o}C) for 24 hours prior to performance testing.

The conversion efficencies for the emission species varied among the oxidation catalysts tested from different vendors. Therefore, the performance of all the oxidation catalysts is not the same for this application. Most oxidation catalysts showed over 90% maximum conversion efficiencies on CO, VOCs and formaldehyde. Saturated hydrocarbons such as propane were difficult to oxidize in a oxidation catalyst due to high activation energy. High VOC oxidation was noticed on all catalysts, with maximum conversion efficiency

at 80%. VOC reduction efficiency was limited by propane emission in the exhaust for the catalyst temperatures tested. Additional formulations need to be developed for oxidation catalysts to increase VOC reduction efficiency. Oxidation of NO to NO_2 was observed on most oxidation catalysts; this reaction is favored based on chemical equlibrium. Variation in space velocity showed very little effect on the conversion efficiencies. Most species showed over 90% conversion efficiency during the space velocity sweep. The oxidation catalysts showed increasing CH_2O conversion efficiency with decreasing space velocity. No change on performance of the oxidation catalysts on conversion of emission species was noticed for varying space velocities after conversion efficiencies reached 90%. Thus, adding more catalyst volume may not increase the reduction efficiency of emission species. Varying cell density showed very little effect on performance of the oxidation catalysts. The friction factor correlation showed the friction factor is inversely proportional to cell density.

ACKNOWLEGEMENTS

First and foremost, I would like to thank my academic advisor, Daniel Olsen for his guidance and support throughout the project. His approach to problems and the ideas he comes up, proved to be of great help in the study. I also thank my committee members, Anthony Marchese and Michael A. De Miranda for their support and guidance throughout the study.

I am thankful to the entire team at the EECL, for their efforts and guidance. I thank my research engineers, Kirk Evans and Cory Kreutzer for their guidance and help throughout the project. Their knowledge on the facility at the EECL was instrumental in the study. I would also like to thank Darryl Beemer, Jason Golly, Adam Friss, Cory DeGroot and Benjamin Neuner for their help in the study. They were always willing to lend their hands when needed.

I thank the department head and staff for their support. I thank Karen Mueller, for her help and support during my time at Colorado State University.

I also would like to acknowledge the sponsors, Pipeline Research Council International (PRCI) for their support. I thank them for giving me an opportunity to work on this project. I also would like to thank the catalyst vendors for providing oxidation catalysts for the study.

Finally, I thank my family and friends for their morale support during the research. Special thanks to my parents K.S. Badrinarayanan and Uma Badrinarayanan for

supporting me throughout my life, providing courage and encouragement. I thank all those, who supported me.

TABLE OF CONTENTS

1. Introduction 1

1.1 Emissions 1

1.1.1 CO Emission 1

1.1.2 NO_x Emissions 3

1.1.3 Hydrocarbon Emissions 4

1.2 Emission Standards 4

1.3 After-Treatment Systems 6

1.3.2 Exhaust Gas Recirculation 6

1.3.3 Particulate Filters 7

1.3.4 Selective Catalytic Reducers 8

1.3.4 Three - Way Catalytic Converter 9

1.3.5 Two - Way Catalytic Converters or Oxidation Catalysts 9

1.4 Oxidation Catalyst Construction 10

1.5 Catalyst Aging and Degreening 14

2. Experimentation 17

2.1 Engine Description 17

2.2 Catalyst Slipstream 19

2.3 Emission Analyzers 21

2.3.1 5-Gas Analyzer 22

2.3.2 Fourier Transform Infra-Red Spectroscopy (FTIR) 24

2.3.3 HP 5890 Series II Gas Chromatograph 25

2.3.4 Varian Gas Chromatograph 32

2.4 Test Procedure 32

2.4.1 Oxidation Catalyst Preparetion 32

2.4.2 Test Plan 34

3. Catalyst Temperature Variation 37

3.1 CO Emission 38

3.2 Formaldehyde Emission 41

3.3 Ethylene Emission 43

3.4 Propylene Emission 44

3.5 Propane Emission 46

3.6 VOC Emission 48

3.6 NO_x Emission 51

4. Space Velocity Variation 54

4.1 CO Emission 54

4.2 Formaldehyde Emission 56

4.3 Ethylene Emission 57

4.4 Propylene Emission 58

4.5 Propane Emission 60

4.6 VOC Emission 61

4.7 NO_x Emission 63

4.8 Friction Factor Correlation 65

5. Conclusion 69

References 72

LIST OF FIGURES

FIGURE 1: VARIATION OF EMISSION CONCENTRATION WITH AIR-FUEL RATIO AND EQUIVALENCE RATIO IN A SPARK IGNITED ENGINE [1] 2

FIGURE 2: STRUCTURE OF CATALYTIC CONVERTER [9] 10

FIGURE 3: EFFECT OF SULPHATING CARRIERS ON METHANE CONVERSION [4] 14

FIGURE 4: EFFECT OF CATALYST AGING ON CONVERSION EFFICIENCIES ON A PD – BASED CATALYST [5] 15

FIGURE 5: EFFECT OF THERMAL AND CHEMICAL AGING ON PT – BASED CATALYST PERFORMANCE [6] 16

FIGURE 6: WAUKESHA VGF-18 GL WITH DYNAMOMETER 17

FIGURE 7: CATALYST SLIPSTREAM SYSTEM 20

FIGURE 8: SCHEMATIC DIAGRAM OF CATALYST SLIPSTREAM 20

FIGURE 9: ROSEMOUNT 5-GAS ANALYZER 22

FIGURE 10: NICOLET FOURIER TRANSFORM INFRA-RED SPECTROMETER 24

FIGURE 11: HP 5890 SERIES II GAS CHROMATOGRAPH 25

FIGURE 12: SCHEMATIC DIAGRAM OF HP 5890 SERIES II GC 26

FIGURE 13: ACTUATION MECHANISM OF 6-PORT VALVE [21] 27

FIGURE 14: GC OVEN TEMPERATURE PROFILE 28

FIGURE 15: GC METHOD TIMETABLE 28

FIGURE 16: CHROMATOGRAM FOR WET EXHAUST SAMPLE FROM VOC GC 30

FIGURE 17: CHROMATOGRAM FOR DRY EXHAUST SAMPLE FROM VOC GC 31

FIGURE 18: PICTURES OF OXIDATION CATALYSTS USED FOR THE STUDY 33

FIGURE 19: MEASUREMENT OF LIGHT-OFF TEMPERATURE FOR EMISSION SPECIES 37

FIGURE 20: VARIATION OF CO CONVERSION EFFICIENCY WITH CATALYST TEMPERATURE 38

FIGURE 21: BRAKE SPECIFIC CO EMISSION VARIATION WITH CATALYST TEMPERATURE.... 40

FIGURE 22: VARIATION OF FORMALDEHYDE CONVERSION EFFICIENCY WITH CATALYST TEMPERATURE 42

FIGURE 23: VARIATION OF ETHYLENE CONVERSION EFFICIENCY WITH CATALYST TEMPERATURE 43

FIGURE 24: VARIATION OF PROPYLENE CONVERSION EFFICIENCY WITH CATALYST TEMPERATURE 45

FIGURE 25: VARIATION OF PROPANE CONVERSION EFFICIENCY WITH CATALYST TEMPERATURE 47

FIGURE 26: VARIATION OF VOC CONVERSION EFFICIENCY WITH CATALYST TEMPERATURE 48

FIGURE 27: BRAKE SPECIFIC VOC EMISSION VARIATION WITH CATALYST TEMPERATURE 50

FIGURE 28: NO_2/NO_X VARIATION WITH CATALYST TEMPERATURE..... 51

FIGURE 29: EQUILIBRIUM CALCULATIONS FOR NO_2/NO_X RATIO AT VARIOUS TEMPERATURES [15] 52

FIGURE 30: VARIATION OF CO CONVERSION EFFICIENCY WITH SPACE VELOCITY 55

FIGURE 31: VARIATION OF FORMALDEHYDE CONVERSION EFFICIENCY WITH SPACE VELOCITY..... 56

FIGURE 32: VARIATION OF ETHYLENE CONVERSION EFFICIENCY WITH SPACE VELOCITY ... 58

FIGURE 33: VARIATION OF PROPYLENE CONVERSION EFFICIENCY WITH SPACE VELOCITY . 59

FIGURE 34: VARIATION OF PROPANE CONVERSION EFFICIENCY WITH SPACE VELOCITY 61

FIGURE 35: VARIATION OF VOC CONVERSION EFFICIENCY WITH SPACE VELOCITY 62

FIGURE 36: VARIATION OF NO_2/NO_x RATIO WITH SPACE VELOCITY 64

FIGURE 37: VARIATION OF DIFFERENTIAL PRESSURE WITH SPACE VELOCITY 66

FIGURE 38: VARIATION OF FRICTION FACTOR WITH REYNOLDS NUMBER 67

LIST OF TABLES

TABLE 1: EMISSION STANDARDS FOR STATIONARY NON-EMERGENCY ENGINES [2] 5

TABLE 2: COMPARISON OF ACTIVE CATALYST MATERIALS 13

TABLE 3: ENGINE SPECIFICATIONS OF WAUKESHA VGF-18 GL 18

TABLE 4: RESULTS TABLE FOR WET EXHAUST SAMPLE FROM VOC GC 30

TABLE 5: RESULTS TABLE FOR DRY EXHAUST SAMPLE FROM VOC GC 31

TABLE 6: CATALYST SPECIFICATIONS 33

TABLE 7: OXIDATION CATALYST TEST PLAN 35

TABLE 8: ACTIVATION ENERGY FOR OXIDATION OF HYDROCARBONS [10] 47

TABLE 9: SUMMARY OF RESULTS FROM THE STUDY 71

1. Introduction

1.1 Emissions

Emissions from IC engines are a major source of air pollution. The exhaust of an engine consists of pollutant emission species like oxides of nitrogen (Nitric oxide (NO) and small amount of nitrogen dioxide (NO_2), collectively known as NO_x), carbon monoxide (CO), carbon dioxide (CO_2) and unburnt (or) partially oxidized hydrocarbons. Diesel engines emit particulate emissions in addition to the above mentioned emission species. In this study, the focus is on emissions from stationary natural gas engines used for power generation, compression and other applications.

Air-fuel ratio, also expressed as equivalence ratio (ϕ) is an important factor in determining the emissions of a SI engine. Aside from racing applications, SI engines operate at stoichiometric or lean air-fuel ratios. The emissions are significantly lower for leaner air-fuel ratios. But at very low air-fuel ratios, the combustion quality reduces due to misfire, increasing CO and hydrocarbon emissions. This creates a need for emission abatement through after-treatment systems. Oxidation catalysts are an important after-treatment system, oxidizing hydrocarbons and CO, reducing the harmful emissions in the engine exhaust. This study was conducted to understand the performance of the oxidation catalysts under different operating parameters, analyzing their effect on performance.

1.1.1 CO Emission

CO emission from an IC engine is controlled by the air-fuel ratio [1]. Figure 1 shows, for rich air-fuel mixtures, CO emission in the exhaust increase rapidly with equivalence ratio, due to the presence of excess fuel. For lean mixtures, the CO emissions are low and

equivalence ratio has very little effect on CO emissions. A SI engine with a three-way catalyst operates close to stoichiometric conditions, requiring high control over the air-fuel ratio to control the emissions.

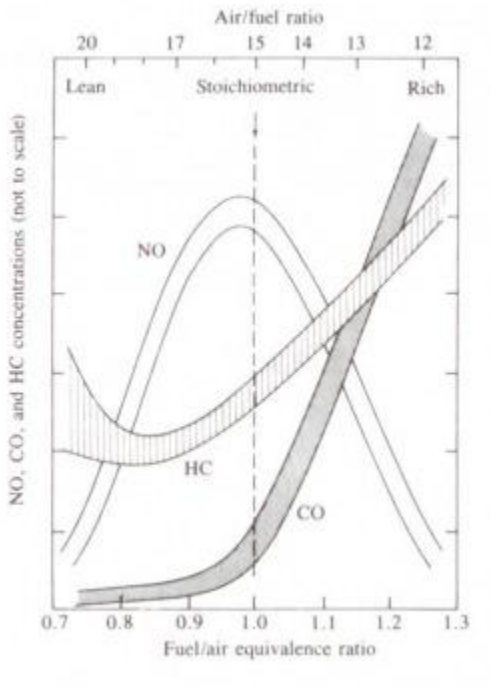

Figure 1: Variation of emission concentration with air-fuel ratio and equivalence ratio in a spark ignited engine [1]

Equation 1.1 shows the principle reaction steps involved in the formation of CO inside an engine cylinder. R, in the equation refers to a hydrocarbon radical.

$$RH \rightarrow R \rightarrow RO_2 \rightarrow RCHO \rightarrow RCO \rightarrow CO \qquad (1.1)$$

1.1.2 NO_x Emissions

Nitric oxide (NO) and nitrogen dioxide (NO_2) are grouped as Nitrogen oxides (NO_x). Nitric oxide is the main constituent of NO_x emitted from most IC engines, produced through the oxidation of nitrogen from the atmospheric air inside the engine cylinder. NO formations have been studied extensively and the mechanism for oxidation of nitrogen at near stoichiometric conditions in a spark ignited engine is widely accepted. Figure 1, presented earlier, shows the trend of NO formation with varying equivalence ratio.

$$N_2 + O \rightarrow NO + N \tag{1.2}$$

$$N + O_2 \rightarrow NO + O \tag{1.3}$$

$$N + OH \rightarrow NO + H \tag{1.4}$$

Equations 1.2 – 1.4 together are commonly known as the Zeldovich Mechanism and are the principle reactions in the formation of NO. The NO formation, according to the mechanism, occurs by the oxidation diatomic nitrogen found in the air inside the combustion chamber at high temperatures. Rate of formation of NO is a function of temperature and residence time inside the engine. The reaction requires high engine temperatures and availability of excess oxygen.

Emitted NO reacts with ammonia and moisture in atmosphere to form nitric acid vapor, which causes acid rain. NO reacts with Volatile Organic Compounds (VOCs) to form ground level ozone, causing lung and respiratory issues.

1.1.3 Hydrocarbon Emissions

Hydrocarbon emissions from an IC engine are a consequence of partial or incomplete combustion of the fuel. Hydrocarbon emissions are collectively known as Total Hydrocarbon (THC) emissions. THC emissions are useful in measuring the inefficiency of combustion inside the engine cylinder. Engine exhaust consists of various hydrocarbon compounds, both inert and highly reactive compounds. Non-methane, non-ethane hydrocarbons are commonly known as Volatile Organic Compounds (VOCs) like propane. The THC emissions group includes VOC emissions. Fuel composition has a significant influence in the composition and quantity of THC and VOC emissions.

Flame quenching close to the engine cylinder wall causes a layer of unburned fuel leading to THC and VOC emission. Fuel trapped in the crevices inside the combustion chamber is also a source of THC emissions. Incomplete combustion inside a cylinder is a common source of THC emissions.

THC emission contributes to smog, a major cause for respiratory diseases. Methane emission, a big contributor to greenhouse effect is difficult to oxidize in the after-treatment systems. VOC emissions cause harmful long term health defects and are dangerous to the environment.

1.2 Emission Standards

Emissions from IC engines are a major cause of environmental and human health issues. Government agencies have developed regulations to control the pollutant emissions from engine exhaust. Emission performance standards provide threshold limits for emission

species. After-treatment systems can be used to reduce pollutant emissions, if they are above the threshold limit.

Table 1 shows the emission standards for natural gas engines based on the manufacture date and rated power. For non-emergency SI natural gas engine, the emission standards are 1 g/hp-hr of NO_x, 2 g/hp-hr of CO and 0.7 g/hp-hr of VOC.

Table 1: Emission Standards for stationary non-emergency engines [2]

Engine type and fuel	Maximum engine power	Manufacture date	Emission standards[a]					
			g/HP-hr			ppmvd at 15% O_2		
			NO_X	CO	VOC[d]	NO_X	CO	VOC[d]
Non-Emergency SI Natural Gas[b] and Non-Emergency SI Lean Burn LPG[b].	100≤HP<500	7/1/2008	2.0	4.0	1.0	160	540	86
		1/1/2011	1.0	2.0	0.7	82	270	60
Non-Emergency SI Lean Burn Natural Gas and LPG.	500≥HP<1,350	1/1/2008	2.0	4.0	1.0	160	540	86
		7/1/2010	1.0	2.0	0.7	82	270	60
Non-Emergency SI Natural Gas and Non-Emergency SI Lean Burn LPG (except lean burn 500=≥HP<1,350).	HP≥500	7/1/2007	2.0	4.0	1.0	160	540	86
	HP≥500	7/1/2010	1.0	2.0	0.7	82	270	60
Landfill/Digester Gas (except lean burn 500≥HP<1,350).	HP<500	7/1/2008	3.0	5.0	1.0	220	610	80
		1/1/2011	2.0	5.0	1.0	150	610	80
	HP≥500	7/1/2007	3.0	5.0	1.0	220	610	80
		7/1/2010	2.0	5.0	1.0	150	610	80
Landfill/Digester Gas Lean Burn	500≥HP<1,350	1/1/2008	3.0	5.0	1.0	220	610	80
		7/1/2010	2.0	5.0	1.0	150	610	80
Emergency	25>HP<130	1/1/2009	[c]10	387	N/A	N/A	N/A	N/A
	HP≥130		2.0	4.0	1.0	160	540	86

Environmental Protection Agency (EPA), manages emission standards across North America. European Union manages the emission standards across Europe. European emission standards are much more stringent and harder to achieve. Current emission standard in Europe is Euro 5, effective since 2010.

1.3 After-Treatment Systems

Engine design, fuel injection and spark timing have improved the engine performance by improving efficiency and reducing emissions. These improvements proved insufficient in meeting many recent emission standards and provide a need for emission after-treatment systems to reduce pollutant emissions. Various after treatment systems have been developed to control the emissions and meet the emission standards.

1.3.1 Secondary Air-Injection System

The primitive and simple after-treatment system developed was a secondary injection of air in to the exhaust stream. The system involved injecting air into the exhaust stream to oxidize the unburned hydrocarbons and CO. The initial methods injected air at the exhaust manifold. The re-combustion of exhaust gases caused damage to exhaust manifold and valves. Another method was to inject downstream of the manifold due to lower exhaust pressure. The exhaust and air mixture flowed through an oxidation catalyst to oxidize CO and hydrocarbons. The inefficiency of these systems led to the development of other exhaust after-treatment systems.

1.3.2 Exhaust Gas Recirculation

Exhaust Gas Recirculation (EGR), is a method of re-injecting exhaust gases into the engine intake for a complete combustion. Injection of exhaust gases into the engine cylinders increases the specific heat of the mixture inside the cylinder, reducing the adiabatic flame temperature. Amount of EGR is dependent on the engine conditions as higher EGR causes misfiring and partial combustion. In a spark ignited engine, generally a maximum of 10 to 15% of exhaust is recirculated into the engine [1]. Typically EGR

reduces NO_x emissions due to reduced combustion temperatures and reduced throttling losses. This causes a compromise on engine performance due to higher charge density inside the cylinder. The recirculation of exhaust can cause clogging at the EGR valves due to the accumulation of particulate matter, requiring more frequent valve maintenance.

1.3.3 Particulate Filters

Particulate filters are trap oxidizers, which effectively reduces particulate emissions. Diesel engines are the major application of particulate filters due to high particulate emissions in the exhaust. The particulate matter is trapped and oxidized on the surface of the temperature tolerant filter. The flow obstruction caused by these trap oxidizers increases pressure in the exhaust. The rise in pressure increases steadily as the particulate matter is accumulated on the trap.

Ignition temperature of the particulate matter is higher than exhaust temperature, requiring controlled combustion to avoid damage or destruction of the trap. The common approach on modern diesel engines is the use of regeneration cycle, operating the engine at rich air-fuel ratio to increase the temperature of the filter to promote oxidation of particulate matter. This operation occurs when the differential pressure across the filter reaches a certain threshold limit. An inlet oxidation catalyst is normally employed to increase NO_2 concentration, which oxidizes PM at a lower temperature.

Ceramic monoliths, alumina coated wire mesh, ceramic fiber mat and silica fiber ropes are the commonly used filters. The application of these filters is depended on the temperature, efficiency and pressure drop. Regeneration of the trap is also important in the selection of the filter for the application.

1.3.4 Selective Catalytic Reducers

Selective catalytic reducers are used to convert NO_x into N_2 and water. A reductant is added to the exhaust stream is absorbed by the catalysts and reduces the NO_x to N_2 and water. Anhydrous or aqueous ammonia and urea are some of the reductants used. Urea is the commonly used reductant due to the toxicity and storage issues of ammonia. The absorbed ammonia reduces NO_x through equations 1.5 to 1.7.

$$4NO + 4NH_3 + O_2 \rightarrow 4N_2 + 6H_2O \quad (1.5)$$

$$2NO_2 + 4NH_3 + O_2 \rightarrow 3N_2 + 6H_2O \quad (1.6)$$

$$NO + NO_2 + 2NH_3 \rightarrow 2N_2 + 3H_2O \quad (1.7)$$

When urea is used, it first undergoes thermal decomposition to form ammonia and CO_2 as a byproduct, followed by reactions in Equations 1.5 to 1.7. The overall reaction of urea with NO is shown in Equation 1.8,

$$4NO + 2(NH_2)_2CO + O_2 \rightarrow 4N_2 + 4H_2O + 2CO_2 \quad (1.8)$$

Ceramic substrates like titanium oxide are commonly used as the substrate for these catalysts in order to tolerate the exhaust temperature and inertness to these reduction reactions. Vanadium oxides, molybdenum oxides, tungsten oxides, zeolites and oxides of precious elements are the common active catalyst materials used in the catalyst. Similar to other after treatment systems, the selection of catalyst material is depended on the exhaust temperature, inertness and thermal degradation of the catalyst. Contamination of the active catalyst materials result in reduced life.

1.3.4 Three - Way Catalytic Converter

A 3-way catalytic converter converts three major emissions of the engine, oxidizing reactions of CO and hydrocarbons and reducing reactions of NO_x. At an air-fuel ratio close to stoichiometric, both CO and hydrocarbon oxidation and NO reduction can be achieved [1]. The air-fuel ratio range is narrow for high conversion efficiencies of all compounds in the three way catalysts. The narrow region of operation is beyond the capabilities of a carburetor. Feedback loops are commonly used in 3-way catalyst systems to overcome the issue of narrow operation range.

The efficiency of the converter is depended on the exhaust temperature, air-fuel ratio and volume and type of catalyst material. An oxygen sensor in the exhaust provides signal to an electronically operated carburetor to control the air-fuel ratio. The ability to oxidize CO and hydrocarbons and reduce NO_x, three way catalytic converters have replaced the conventional oxidation catalysts, which are still effective on lean burn engines.

1.3.5 Two - Way Catalytic Converters or Oxidation Catalysts

Two way catalytic converters or oxidation catalysts oxidize CO and HCs into CO_2 and water simultaneously. The oxidation catalyst is a common after treatment approach in most lean burn natural gas engines due to high carbon based emissions. Diesel engines are also common application for oxidation catalysts for oxidation of CO and hydrocarbons due to excess oxygen in exhaust. About half the emissions in a natural gas engine exhaust are unburned hydrocarbons including methane, ethane and partially oxidized hydrocarbons. About 25% of the exhaust is saturated hydrocarbons, which are difficult to oxidize. Lean burn engines contain excess oxygen in the exhaust, enabling easier oxidation of CO and THCs [1]. The oxidation catalyst enables the reactions in the

Equations 1.9 and 1.10 for the oxidation of CO and THC. The rates of these reactions follow Arrhenius form. Therefore, the reactions are exponentially dependent on catalyst temperatures. NO_x emissions can also have an effect on oxidation of THCs.

$$2CO + O_2 \rightarrow 2CO_2 \quad (1.9)$$

$$C_xH_{2x+2} + [(3x+1)/2]\ O_2 \rightarrow xCO_2 + (x+1)\ H_2O \quad (1.10)$$

1.4 Oxidation Catalyst Construction

The two – way catalytic converter consists of three components, a substrate, wash coat and active catalyst material. A microscopic view of the structure of catalytic converter is shown on Figure 2. The figure shows the structure of catalyst substrate and wash coat in an oxidation catalyst.

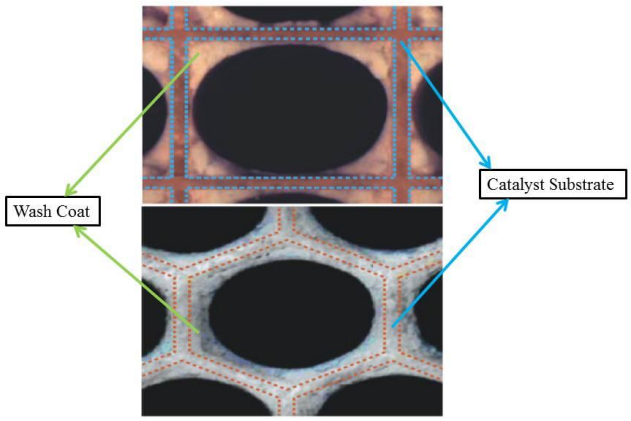

Figure 2: Structure of catalytic converter [9]

Catalyst Substrate: A ceramic monolith with a honeycomb structure is a common substrate used in oxidation catalysts. Metallic substrates are also used in some applications. Ceramic cores are inexpensive and tolerant to high temperatures. Catalyst

substrates are designed to provide a high surface area to support the catalyst wash coat. The substrate is also designed to avoid excessive pressure drop across the converter.

Wash Coat: A wash coat is a carrier for the active catalyst materials and is used to disperse the materials over a high surface area. Aluminum oxide, Titanium dioxide, Silicon dioxide, or a mixture of silica and alumina are common carrier materials used in oxidation catalyst. The active catalyst materials are suspended in the wash coat before deposition on the core. Wash coat materials form a rough, irregular surface, which increases the surface area compared to the smooth surface of the bare substrate. This maximizes the active surface available for oxidation of CO and THC in the engine exhaust.

Active Catalyst Material: The catalyst material is most often a precious metal. Platinum, palladium, rhodium and other precious metals are commonly used active catalyst material. Cerium, iron, manganese and nickel are also used, although each has its own limitations.

The catalyst materials are selected based on the abilty to store oxygen. The active catalyst material oxidizes and stores excess oxygen. It releases the stored oxygen for the oxidation of CO and THC. The wash coat, consisting of oxides, can also store and release oxygen, similar to active catalyst material.

Pt – based and Pd – based catalysts have been researched extensively to understand their performance. Pd – based catalyst show better oxidation activity compared to other active catalyst metals [4]. Pt-Pd bimetallic catalysts show excellent activity of THC oxidation [3].

No (or) very little activity can be seen on NO_x emissions on all catalyst materials. Performance of oxidation catalysts are depended on catalyst temperatures.

The Pt/Pd –based catalyst perform similar to the Pd – based catalyst with good THC conversion efficiencies. Pt – based catalysts show inefficiency in THC oxidation. THC conversion efficiencies on Pt/Pd and Pd – based catalyst is near 100% at temperature range of 350 to 600^{o}C, providing a wider range of operation. Pt – based catalyst material has maximum conversion efficiency of 80% at 600^{o}C.

Pd - based catalysts are prone to sulpahte posioning. The PdO would form inactive $PdSO_4$, in the presence of SO_2 [3], causing deactivation of active catalyst material. Pt – based catalysts are not sensitive to sulphur poisoning, but are not as active as Pd – based catalysts in THC oxidation. Figure 4 also shows the effect of poisoning on the performance oxidation catalysts. Sulphur poisoned and aged catalysts (described later in the chapter) cause drop in efficiency due to loss of active catalyst material.

The comparison of commonly used active catalyst material is shown in Table 2. Pt – based catalysts deactivate at a slower rate, but less active on oxidation of CO and hydrocarbons.

Table 2: Comparison of active catalyst materials

Catalyst Material	Advantages	Disadvantages	Comments
Pt - based Catalyst	• Resistant to poisoning • Slower deactivation	• Low conversion efficiency	• Longer catalyst life • Low conversion efficiency
Pd - based Catalyst	• Higher conversion efficiencies • Near 100% oxidation of CO	• Prone to poisoning • Deactivates faster than other catalyst material	• Very good conversion efficiency • Deactivates faster
Pt-Pd based Catalyst	• Resistant to sulphate poisoning • Good conversion efficiencies	• Low NO conversion efficiency	• Better conversion efficiency than Pt-based catalysts • Deactivates slower than Pd catalyst

Pd – based and Pt/Pd – based catalyst show good conversion efficiencies of CO and hydrocarbons, but deactivates faster. Pt/Pd – based catalysts are newly developed compared to other active catalyst material. Extensive research are done to understand the effect of concentrations of Pt and Pd on performance of these catalysts.

Carrier (or) wash coat also affects the poisoning of active catalyst materials. Sulphating carriers allow slower deactivation of the catalyst due to sulphur poisoning. Figure 3 shows the effect of sulphating support on the oxidation of methane. Supports like alumina react with SO_2 in the exhaust forming aluminum sulphate.

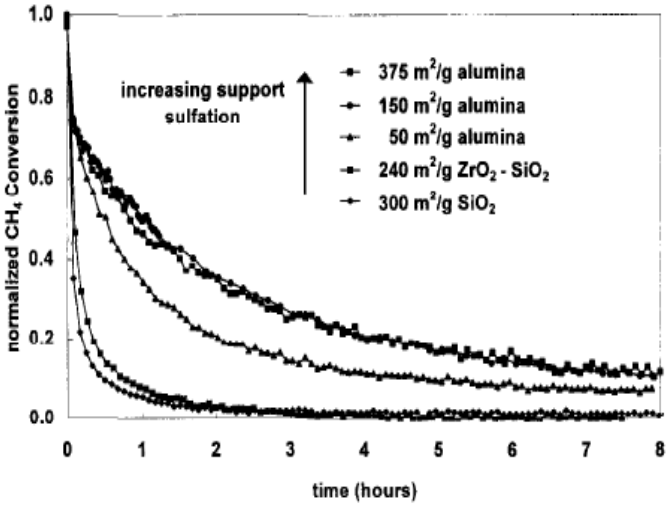

Figure 3: Effect of sulphating carriers on methane conversion [4]

The posisonig of carrier allows slower deactivation of the catalyst. Higher carrier concentration can also aid in slower deactivation of oxidation catalysts. Carriers like silicon dioxide and zirconium dioxide are not sensitive to sulphate poisoning, deactivting the catalyst at a faster rate [3].

1.5 Catalyst Aging and Degreening

Long term durability of catalysts is affected by thermal and chemical aging processes. Thermal aging can cause sintering, decreasing the catalytic activity of the precious metal. Sintering can also cause destructuring of wash coat, encapsulating active catalyst material[5]. Chemical aging process causes blockage of channels, covering active catalyst materials.

Degreening is the intial drop in efficiency, when a new catalyst is place in the engine exhaust. Degreening is caused by various parameters, commonly initial sintering and

chemical binding. The mechanism is not considered as a aging process and studies are done to understand the process and developing methods to reduce the drop in efficiency.

Thermal and chemical aging are the major cause for drop in efficiency. Figure 4 and 5 show the effect of aging process on catalyst performance. The rate of drop in efficiency is affected by the thermal aging temperature as shown in Figure 4. Conversion efficiency of oxidation catalysts aged at a higher temperature decreases at a faster rate.

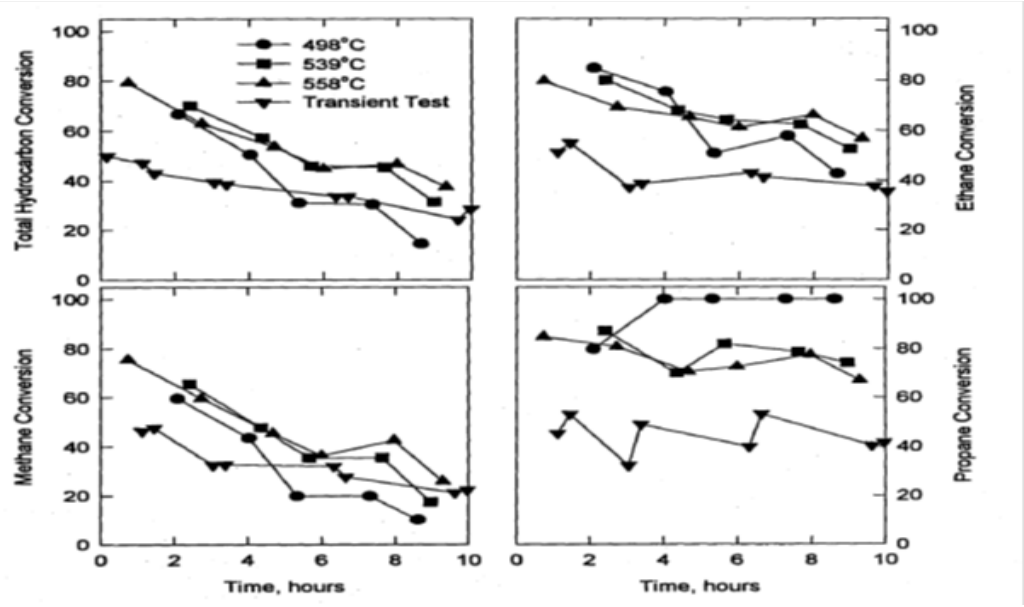

Figure 4: Effect of catalyst aging on conversion efficiencies on a Pd – based catalyst [5]

Aging causes efficiency drop at a higher temperature compared to a fresh catalyst as seen on Figure 4. Thermal aging can also have effects on NO_x emissions as seen on Figure 5.

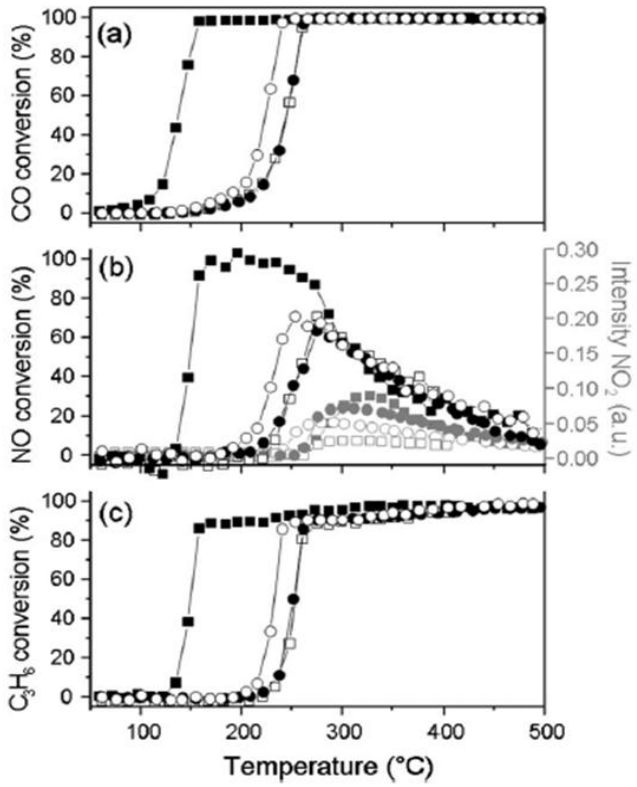

Figure 5: Effect of thermal and chemical aging on Pt – based catalyst performance [6]

Chemical aging can be caused by sulphur poisoning and studies are performend to abate the mechanism. Phosphate posioning and structural changes are also the effects of aging processes.

2. Experimentation

The components for the experimental testing of oxidation catalysts are installed at the Engines and Energy Conversion Lab (EECL) of Colorado State University. A portion of the exhaust from the Waukesha VGF-18 GL was used to supply the catalyst slipstream. Exhaust slipstream system was originally designed and fabricated by Enviro Kinetics, Inc with some modifications which were done at the EECL. The functiom of the slipstream is to control the operational parameters of the oxidation catalyst. Emission analyzers were used to measure the concentrations of emission species.

2.1 Engine Description

Waukesha VGF-18 GL is a 4-stroke stationary lean burn natural gas engine. The engine has 6 in-line cylinders with a total displacement of 18 litres. Figure 6 shows the Waukesha VGF-18 GL engine on a test rig at the EECL.

Figure 6: Waukesha VGF-18 GL with dynamometer

The bore of the cylinder and the stroke of the piston is 9.35 and 8.5 inches respectively. The engine operates at the rated load of 300 kW and at a rated speed of 1800 rpm. The engine specifications are shown in Table 3.

Table 3: Engine Specifications of Waukesha VGF-18 GL

Engine Specifications	
Manufacturer	Waukesha
Model	VGF-18 GL
Type	Lean burn natural gas engine
Number of Cylinders	6 In-line
Rated Load	300 kW
Rated Speed	1800 rpm
Ignition System	Spark Ignited
Bore	9.35 inches
Stroke	8.5 inches

A Garner-Denver screw compressor supplies air to the engine at the desired pressure. In this study, sea level pressure of 101.3 kPa was supplied, boosted from approximately 84 kPa at the site altitude of 1525 m. A exhaust back pressure valive controls the engine back pressure to the aire supply. The engine operates on natural gas supplied to the building. The natural gas supply line includes a propane injection system, allowing propane concentration in the fuel to be increased. The propane injection was controlled to maintain 5 to 10 ppm propane concentration in the exhaust. For further details on the engine specification please review Masters thesis of Kristopher Quillen [12].

2.2 Catalyst Slipstream

The slipstream system allows engine exhaust to flow through it, enabling control over catalyst operating parameters for research purposes. The slipstream system consists of a liquid-gas heat exchanger and flow control valve, enabling control of temperature and space velocity. Original design by Enviro Kinetics consisted of a gas-gas heat exchanger. Residence time is an important operational parameter for catalysts. The time spent by the exhaust inside a catalysts is known as residence time. Residence time is often referred in the form of space velocity, which is inverse of residence time in units of hr^{-1}. Slipstream enables the catalyst operating parameters to be independent of engine parameters.

Figure 7 shows the catalyst slipstream, which was connected to the engine exhaust stream through stainless steel flexible tubes which were thermally insulated. Figure 8 shows the schematic diagram of catalyst slipstream system. The engine exhaust is diverted to the bottom half of the slipstream as shown in Figure 8. The bypass control valve controls the flow rate through the heat exchanger, allowing control over catalyst temperature. Engine coolant was pumped into the heat exchanger to control the temperature of the exhaust. A labview program was developed to control the bypass valve position for a desired catalyst temperature setpoint.

Figure 7: Catalyst slipstream system

The other flow control valve downstream of the heat exchanger was used to control the entire flow through the system, controlling the space velocity. A secondary control loop on the labview program controlled the position of the space velocity control valve.

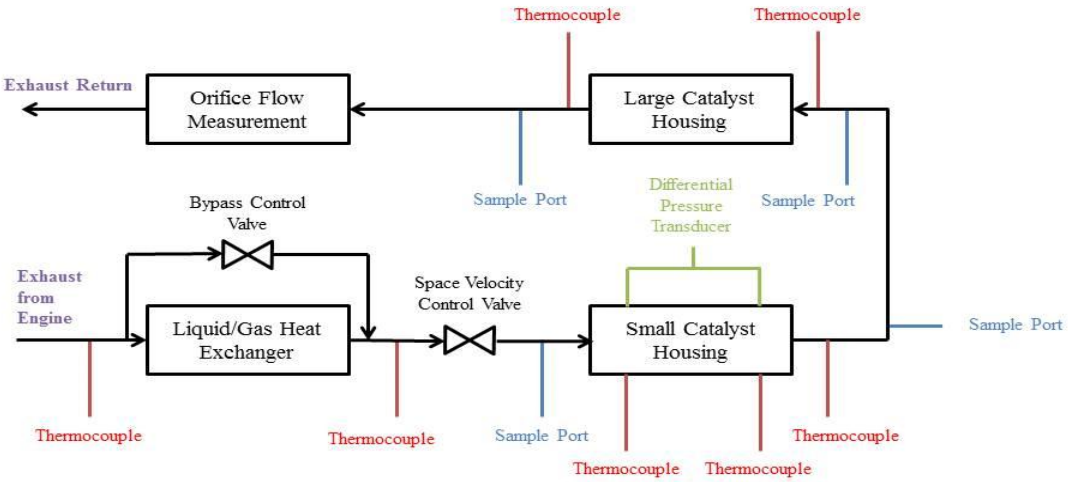

Figure 8: Schematic diagram of catalyst slipstream

The flow rate through the system is measured by a orifice flow measurement at the end of the slipstream. The space velocity was computed using the overall flowrate through the system and the catalyst envelope volume. The catalyst slipstream consists of two different catalyst housings, a small (0.152 m x 0.165 m x 0.482 m) housing and a large (0.152 m x 0.165 m x 1.473 m) housing. The cross section of the housing is slightly larger than that of the oxidation catalyst. The small catalyst housing was used for the study, due to the small sized oxidation catalysts. For the measurement of catalyst temperatures, Omega K-type grounded thermocouples were placed across the catalyst housing as shown in Figure 9. The thermocouples were grounded for accurate temperature measurements and toleranance to high exhaust temperatures upto a maximum of 1650^{o}F (900^{o}C). The thermocouples were placed within 1 inch of the catalyst surface for accurate catalyst temperature measurements. A Rosemount differential pressure transducer with a 0 to 55 inches of water (0 to 0.136 bar) range was used to measure the pressure drop across the catalyst. The entire system, until the end of catalyst housing was thermally insulated using fiberglass insulation. Insulation allowed better control over exhaust temperature and increased maximum catalyst temperature.

For more details on the construction of catalyst slipstream system, review the Masters thesis of Joshua C. Schmitt [11].

2.3 Emission Analyzers

Emission measurement is an important part of the project and three different emission analyzers were used, specializing in specific emission species.

2.3.1 5-Gas Analyzer

The Rosemount 5-gas emission measurement bench has the capability of measuring 5 different emission species. The analyzer measures concentrations of CO, CO_2, NO_x, THC and O_2. The analyzer uses dry sample to measure these emission species. The exhaust sample flows through a peltier type condenser which removes water from the exhaust. Figure 9 shows the Rosemount 5-gas analyzer in the control room at EECL.

Figure 9: Rosemount 5-Gas analyzer

Emission species like CO and CO_2 are sensitive to infra-red radiation. These emission species are excited at certain wavelengths of infra-red radiation. The radiation absorption profile is used to quantify concentrations of CO and CO_2.

THC emissions are measured by a Flame Ionization Detector (FID). The detector uses ions to calculate the THC concentrations. The source of these ions is a small hydrogen-air flame that pyrolyzes the hydrocarbons in the sample producing positvely charged ions and electrons. Electrodes with a potential difference are used to detect the ions. The ions are attracted towards the electrode surface causing flow of current. The measured current is used to quantify the emission concentration.

The 5-gas analyzer uses chemiluminecense for measurement of NO_x in the exhaust sample. The chemiluminecense method measures the NO_x concentration via equations 2.1 to 2.3.

$$NO_2 \rightarrow NO + 1/2O_2 \quad (2.1)$$

$$NO + O_3 \rightarrow NO_2^* + O_2 \quad (2.2)$$

$$NO_2^* \rightarrow NO_2 + Photon \quad (2.3)$$

All NO_x species are reduced to NO across the catalysts. The reduced NO passes through a chamber containing ozone, forming NO_2 in an excited state. The NO_2 molecules return to ground NO_2 by releasing a photon. The emitted light is measured using a photo diode and the amount of photons released.

Oxygen concentration in the exhaust is measured based on the magnetic susceptability of the gas sample. Diatomic oxygen molecules have much higher magnetic susceptability than other gases in the exhaust. The 5-gas analyzer was connected to a LabView® program which recorded the data. The analyzer contains a built-in display that shows measurements real time.

2.3.2 Fourier Transform Infra-Red Spectroscopy (FTIR)

Government agencies have described some hydrocarbons as highly toxic. These hyrocarbons are referred to as Hazardous Air Pollutants (HAPs). Formaldehyde, acetaldehyde and acrolein are some of the HAPs, requiring accurate measurements due to their low emission concentrations. Figure 10 shows the FTIR in the control room at the EECL.

A Nicolet Fourier Transform Infra-Red (FTIR) spectrometer is used for the measurement of HAPs in the engine exhaust. Similar to CO and CO_2 emission measurement in the 5-gas analyzer, FTIR uses infra-red radiation absorption mechanism to measure HAPs concentration. FTIR scans the exhaust sample with infra-red radiation at various wavelengths. It measures the absorption at various wavelengths to determine the concentrations of various emission species. All polar molecules absorb infra-red radiation at one (or) more wavelengths.

Figure 10: Nicolet Fourier Transform Infra-Red Spectrometer

As shown in Figure10, FTIR uses a heated sample line. Heated sample lines allow wet measurement of species, preventing water condensation in the line that can absorb emission species soluble in water.

2.3.3 HP 5890 Series II Gas Chromatograph

Measurement of individual VOCs is important to understand the performance of the oxidation catalysts. HP 5890 series II GC was used to measure VOCs with low detection limits, down upto 10 ppb. Figure 11 shows the HP 5890 series II GC in the control room at the EECL.

Figure 11: HP 5890 Series II Gas Chromatograph

Flame Ionization Detector (FID) was used by the GC to measure VOCs. The working principle of the detector was explained in previous section 2.3.1. Figure 12 shows the schematic diagram of GC operation. The flow between calibration gas and exhaust sample was controlled by a manually actuated 3-way valve. A heated sample line was used for the sample gas to avoid miscibility of emission species in water. The pressure of

the sample inlet was monitered using a pressure gauge. The sample inlet pressure was regulated by a relief valve at the downstream of the pressure gauge. The flow through the capillary column is controlled by a 6-port valve. The valve is a 4-way valve as shown in Figure 14.

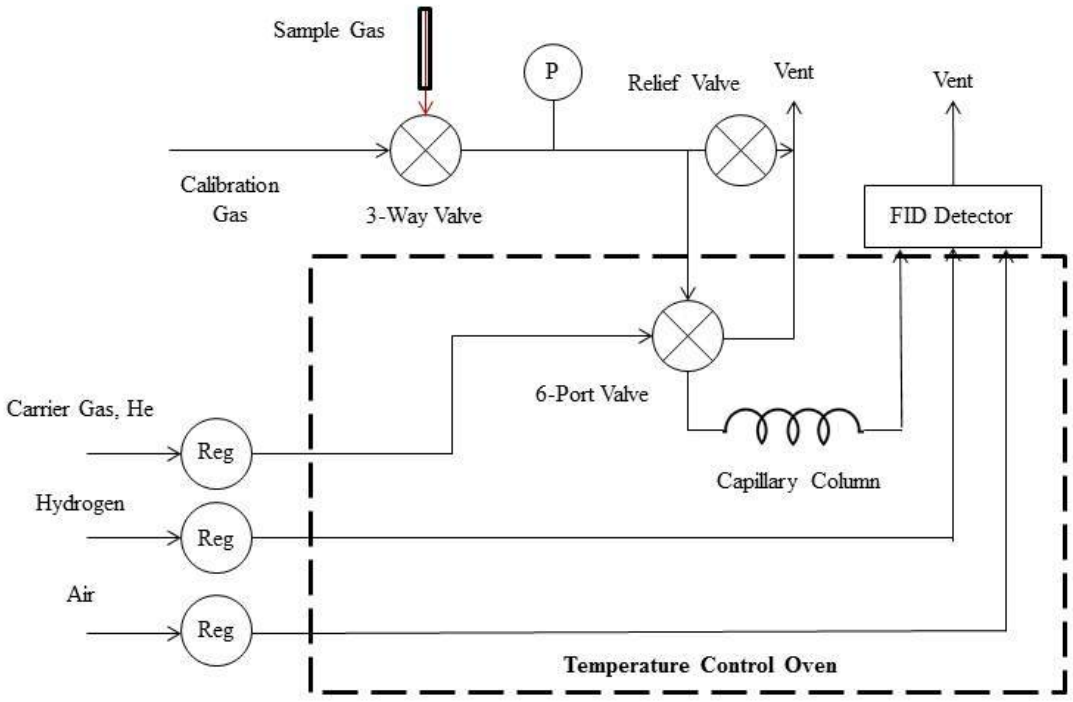

Figure 12: Schematic diagram of HP 5890 Series II GC

The 6-port valve controls the flow through the capillary column, which leads to the FID. The hydrogen and air flow needed to sustain the FID flame are regulated individually. It is important to regulate them individually to avoid uncontrolled combustion of the fuel.

Figure 13 shows the actuation mechanism of the 6-port valve. The valve is actuated at the start of the run. At ON position, the valve allows sample gas to flow through the pre-column into the vent. At OFF position, the valve allows flow of carrier gas to the detector

through the pre-column. The valve was actuated from ON to OFF position at the start of the run. The exhaust sample trapped inside the pre-column is pushed to the detector by the carrier gas.

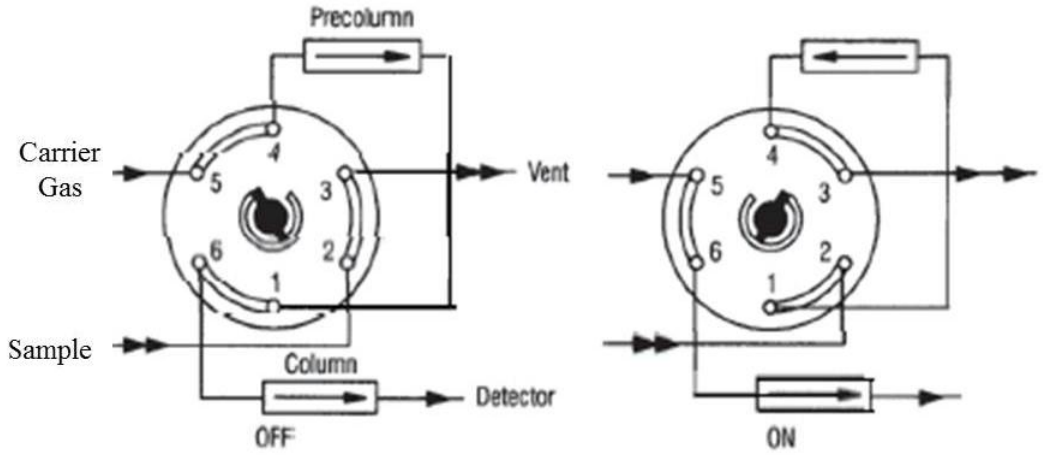

Figure 13: Actuation mechanism of 6-port valve [21]

The GC uses a Agilent Plot Q capillary column which was 30 m long and 0.5 mm diameter. The part number for the column is 19091P-QO4 available at www.agilent.com. The main function of the capillary column is to separate the emission species individually. The seperation of emission species is achieved by the oven temperature profile, based on their molecular weight. The plot Q column was capable of seperating apolar and polar molecules.

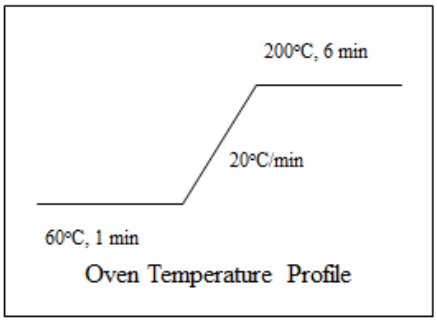

Figure 14: GC oven temperature profile

Figure 14 shows the temperature profile of the GC oven. At the start of the run, the temperature of the oven is maintained at 140^{o}F (60^{o}C) for 1 minute. The temperature is then ramped upto 390^{o}F (200^{o}C) at the rate of 70^{o}F/min (20^{o}C/min). The temperature is maintained at 200^{o}C till the end of the run. Maintaining high oven temperature at the end burns off any residue in the column and allows fresh sample to enter at the start of next run.

The GC was controlled and operated on a computer using Clarity software. Figure 15 shows the timetable for GC operation method that was developed on the Clarity software. The GC operation method was developed on the clarity software based on the temperature profile.

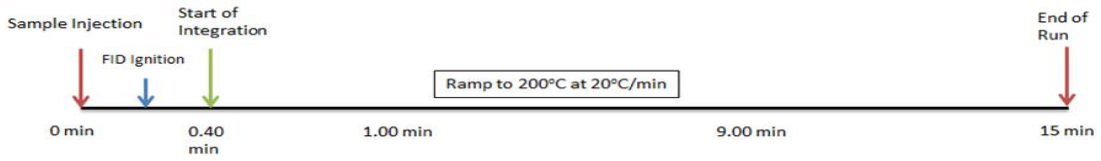

Figure 15: GC method timetable

The exhaust sample injection occurs at the start of the run. Ignition of FID flame and start of integration are achieved within 30 seconds from start of run. During the run, the clarity software record the data in the form of chromatograms, which are integrated into emission concentration.

The GC was operated with wet exhaust samples. Tests conducted on dry samples showed loss of emission species due to their missibilty in water. Figures 16 and 17 show the wet and dry sample chromatograms from the GC. Tables 4 and 5 show the results table for wet sample from the GC. Emission species like ethylene and ethane have low exhaust concentrations on dry samples, due to their missibility in water.

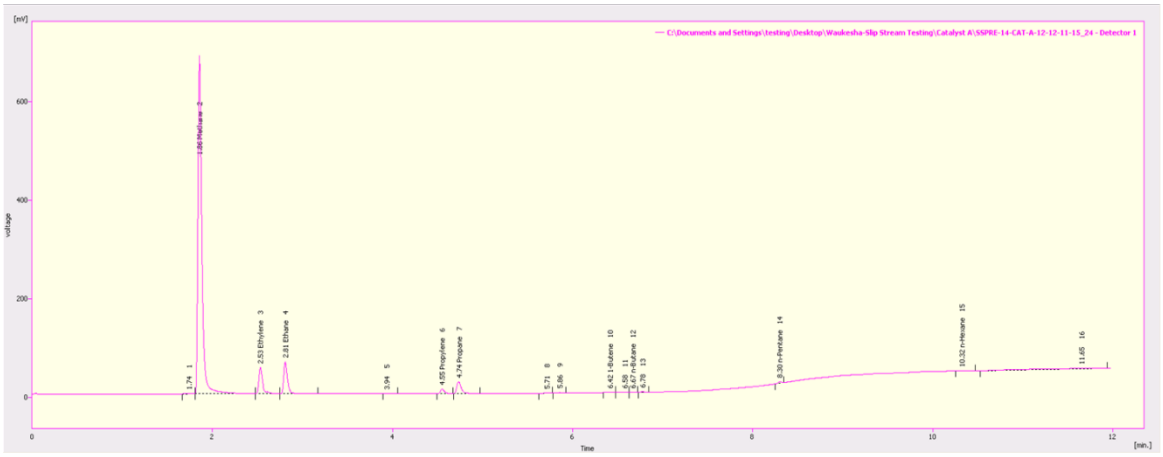

Figure 16: Chromatogram for wet exhaust sample from VOC GC

Table 4: Results table for wet exhaust sample from VOC GC

Peak No.	Retention Time (min)	Response	Amount (ppm)	Amount (%)	Peak Type	Compound Name
2	1.857	2009.530	559.229	90.3	Ordnr	Methane
3	2.530	155.161	22.631	3.7	Ordnr	Ethylene
4	2.807	183.112	26.353	4.3	Ordnr	Ethane
6	4.550	28.020	2.341	0.4	Ordnr	Propylene
7	4.737	81.934	7.989	1.3	Ordnr	Propane
10	6.417	1.191	0.070	0.0	Ordnr	1-Butene
12	6.670	1.113	0.066	0.0	Ordnr	n-Butane
14	8.300	7.945	0.341	0.1	Ordnr	n-Pentane
15	10.323	1.800	0.046	0.0	Ordnr	n-Hexane
	Total		619.067	100.0		

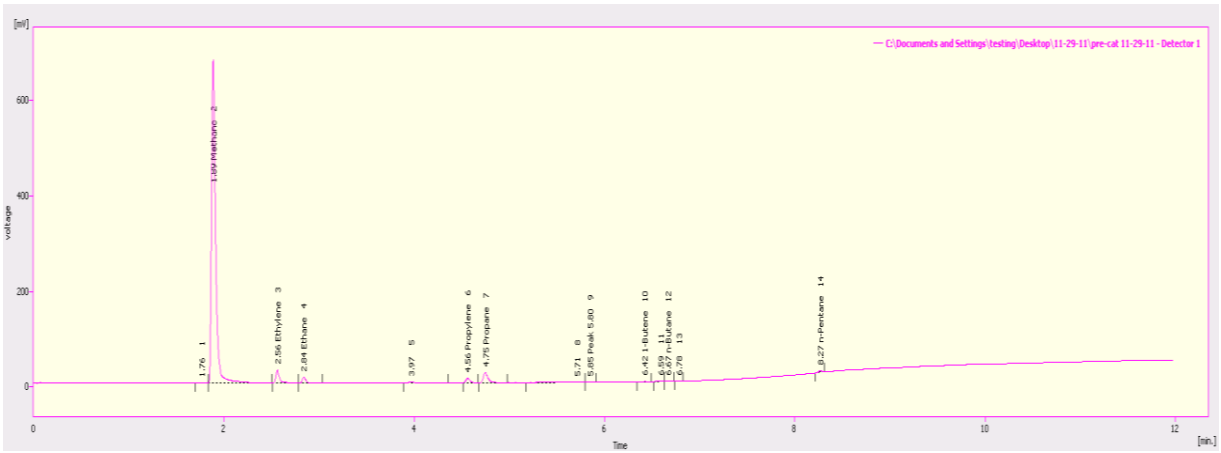

Figure 17: Chromatogram for dry exhaust sample from VOC GC

Table 5: Results table for dry exhaust sample from VOC GC

Peak No.	Retention Time (min)	Response	Amount (ppm)	Amount (%)	Peak Type	Compound Name
2	1.8887	1962.401	546.114	95.3	Ordnr	Methane
3	2.560	79.876	11.527	2.0	Ordnr	Ethylene
4	2.837	32.823	4.666	0.8	Ordnr	Ethane
6	4.560	27.465	2.702	0.5	Ordnr	Propylene
7	4.750	74.603	7.206	1.3	Ordnr	Propane
10	6.423	1.420	0.108	0.0	Ordnr	1-Butene
12	6.667	1.775	0.134	0.0	Ordnr	n-Butane
14	8.267	8.339	0.410	0.1	Ordnr	n-Pentane
15	10.335					n-Hexane
	Total		572.866			

An Air Dimensions micro sized heated head pump was used to pump the wet exhaust sample to the GC to maintain the sample flow rate into the GC. The sample inlet pressure was maintained at 15 psi using the pressure relief valve.

2.3.4 Varian Gas Chromatograph

It is necessary to know the fuel composition to calculate the Brake Specific Emissions (BSE). The Varian micro gas chromatograph was used to measure fuel composition. The GC uses a thermal conductivity detector for the measurements of hydrocarbons in the fuel.

The GC consists of a two channel micro sized valve, column and detector, allowing measurements on small sample quantities in short analysis times (less than 2 minutes). GC control and species quantification were carried out using Galaxie software.

2.4 Test Procedure

The testing was conducted at the EECL. The slipstream system was connected to the engine exhaust. A heated sample line was used to flow exhaust to the emissions analyzers. A manually actuated valve was used to switch between pre-catalyst sample and post-catalyst sample.

Five different oxidation catalysts were evaluated in the study. Performance of oxidation catalysts for varying catalyst temperature and space velocity was measured.

2.4.1 Oxidation Catalyst Preparetion

Five commercial catalyst vendors provided oxidation catalysts for performance analysis. The oxidation catalysts were subject to preparetion processes, enabling comparison between the catalysts. Degreening of oxidation catalysts is a concept that is not well understood. Different oxidation catalysts have different degreening rates and temperatures. It is necessary to degreen the catalysts before analyzing their performance, ensuring emission destruction efficiencies are stable.

Figure 18 shows the images of the oxidation catalysts that were used for the study. All the oxidation catalysts were degreened at a temperature of 1200^{o}F (650^{o}C) for 24 hours. The catalysts were degreened in a kiln at the EECL. Table 6 shows the specifications for oxidation catalysts tested. The envelope volume or the flow volume varied significantly among the oxidation catalysts. Significant variations in cell density of the oxidation catalysts was observed. The catalyst dimensions and specifications were measured for calculation and analysis purposes.

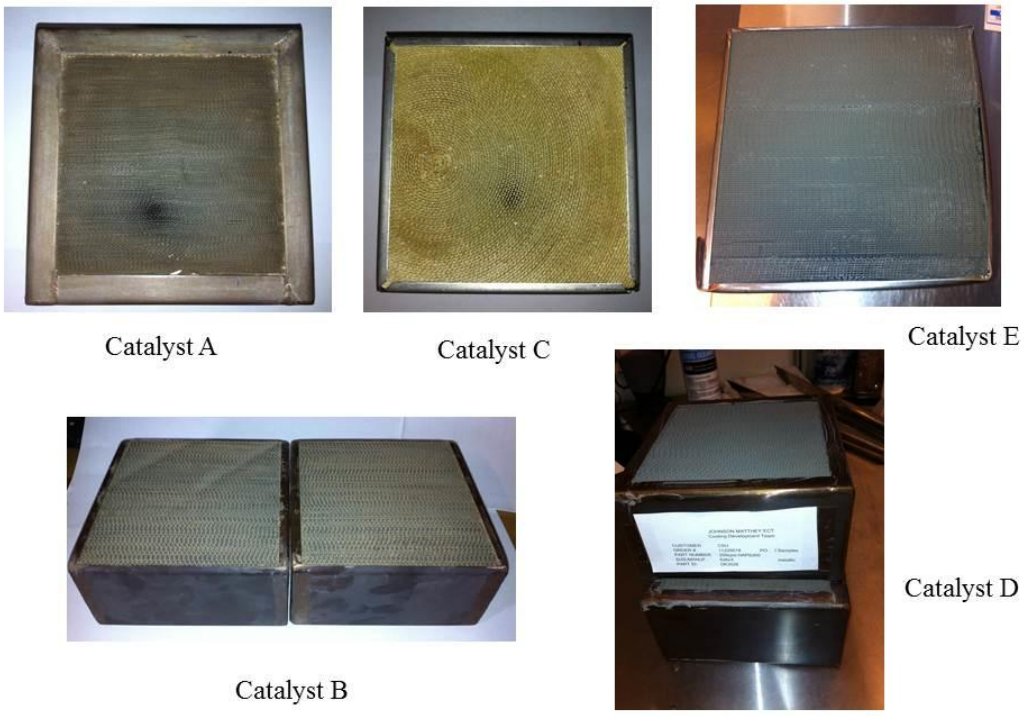

Figure 18: Pictures of oxidation catalysts used for the study

Table 6: Catalyst specifications

Table 7: Catalyst specifications

Specifications	Catalyst - A	Catalyst - B	Catalyst - C	Catalyst - D	Catalyst - E
Module Length (inches)	5.689	5.880	5.978	6.38	7.075
Module Width (inches)	5.953	5.872	6.017	5.902	7.332
Module Height (inches)	5.982	5.855	5.981	5.897	6.328
Module Volume ($inch^3$)	202.60	202.710	215.134	222.57	328.258
Envelope Length (inches)	5.422	5.600	5.776	6.101	6.997
Envelope Width (inches)	4.684	5.481	5.419	4.851	5.67
Envelope Height (inches)	4.714	5.262	5.369	4.842	5.615
Envelope Volume ($inch^3$)	119.73	161.700	168.080	143.12	222.768
Cell Density ($cells/inch^2$)	600	300	300	200	300
Degreening Temperature (^oC)	650	650	650	650	650
Degreening Time (hrs)	24	24	24	24	24

2.4.2 Test Plan

The oxidation catalysts received from the vendors were tested for the performance under different operating conditions. The catalysts were degreened and their conversion efficiencies was measured using the slipstream system. The performance of the oxidation catalysts were tested for varying exhaust temperature and space velocity.

The activation energy required for oxidation of hydrocarbons in the exhaust is provided by the heat. Therefore, catalyst temperature is critical in understanding the performance of the oxidation catalyst. Table 7 shows the test plan for the study used to performe temperature and space velocity sweep.

Table 8: Oxidation catalyst test plan

Day	Catalyst Module	Temperature	Space Velocity
1	A	300-800°F at 150k hr^{-1}	Sweep at 550°F
2	B	300-800°F at 150k hr^{-1}	Sweep at 550°F
3	C	300-800°F at 150k hr^{-1}	Sweep at 550°F
4	D	300-800°F at 150k hr^{-1}	Sweep at 550°F
5	E	300-800°F at 150k hr^{-1}	Sweep at 550°F

Pre-catalyst data were recorded before performing the temperature sweep on the oxidation catalysts. The catalyst temperature was maximized by by-passing the heat exchanger in the catalyst slipstream system. The exhaust temperature was reduced at a rate of about 2^{o}F/min. The emissions were continually measured using the analyzers until minimum exhaust temperature was achieved by the heat exhanger. During the run, the space velocity was maintained at 150,000 hr^{-1}. At the end of the temperature sweep, the pre-catalyst emissions were recorded to confirm stable exhaust conditions.

The other important parameter used for catalyst specification is residence time of the exhaust. The time spent by the exhaust inside the catalyst module is known as residence time. Residence time is often shown in the form of space velocity, which is the inverse of residence time in units of hr^{-1}. Similar to temperature sweep, the space velocity of the catalyst was varied from maximum to minimum by the flow control valve in the slipstream system. The emission analyzers were operated continuously during the sweep. The exhaust temperature during the run was maintained at 550^{o}F. The performance of the

oxidation catalysts during temperature and space velocity sweep is are discussed in the following chapters.

3. Catalyst Temperature Variation

The catalyst performance is significantly affected by catalyst temperature. Generally, the reaction rate across the catalyst follows Arrhenius form, exponentially increasing with temperature. The activation energy required for oxidation of CO and hydrocarbons is reduced by activation sites in the catalyst. Figure 19 shows the variation in concentration and conversion efficiency of CO for catalyst A.

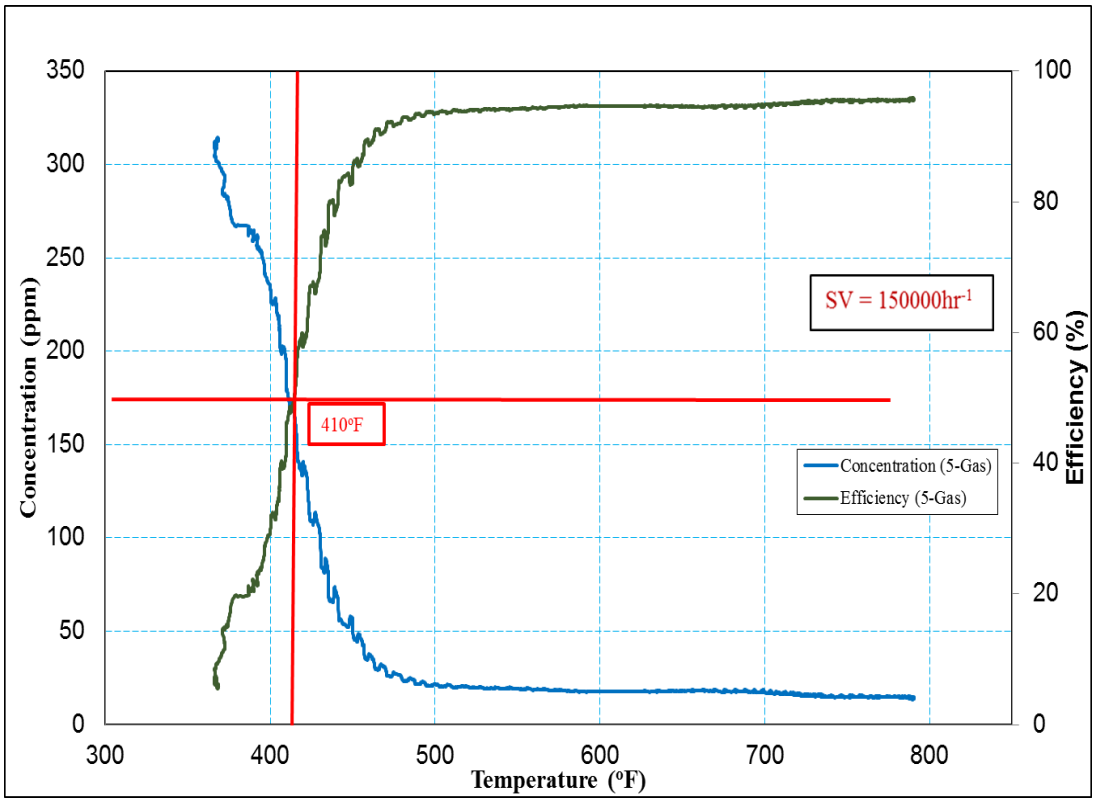

Figure 19: Measurement of light-off temperature for emission species

The conversion efficiency of emission species were measured using the formula shown in Equation 3.1.

$$\text{Conversion efficiency} = \frac{1 - \text{Post-catalyst mole faction}}{\text{Pre-catalyst mole fraction}} * 100\% \qquad (3.1)$$

The performance of the oxidation is often referred in terms of light-off temperature. Light-off temperature is defined as the temperature at which the conversion efficiency of an emission species decreases to 50% [14]. As shown in Figure 19, 50% of maximum conversion efficiency for CO in catalyst A was 46%. The light off temperature for oxidation of CO on catalyst A was 410°F (770°C).

3.1 CO Emission

As discussed earlier, CO emission is the major component in lean burn natural gas engine exhaust. The CO emission abatement is critical to meet the emission standards. Figure 20 shows the performance of the oxidation catalysts on CO conversion.

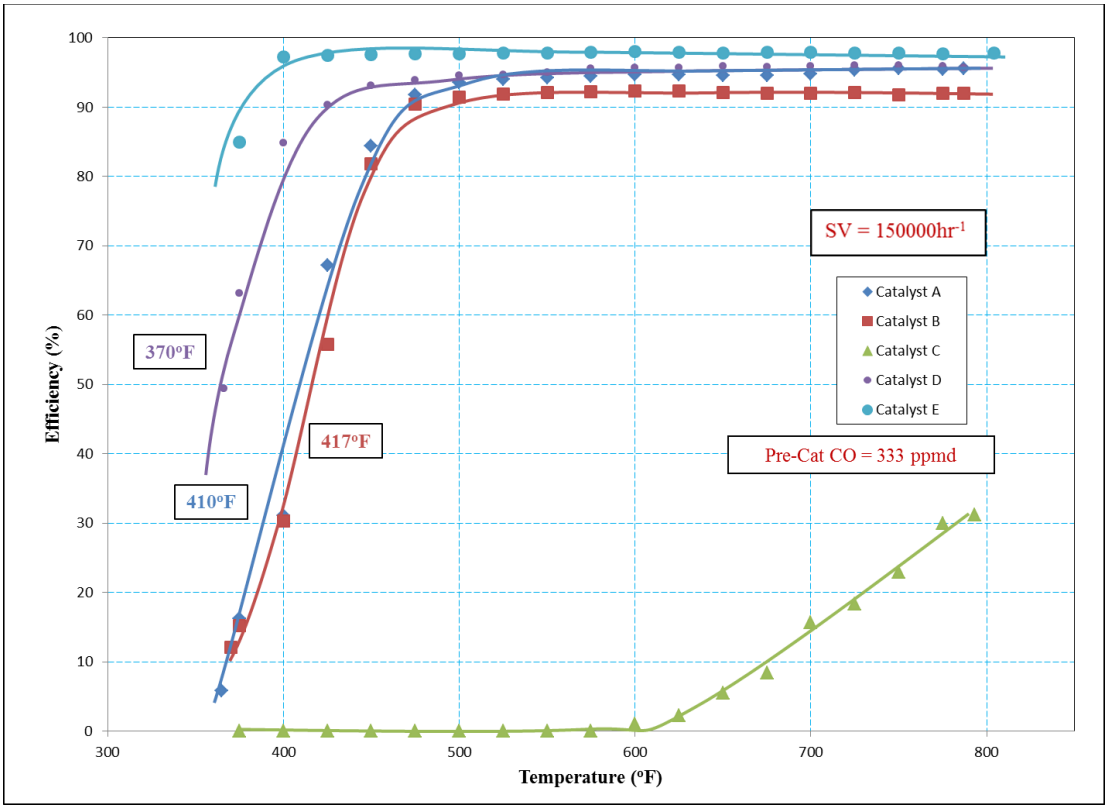

Figure 20: Variation of CO conversion efficiency with catalyst temperature

Pre-catalyst CO emission was measured at 333 ppm by the 5-gas analyzer. Most catalysts showed CO conversion efficiencies sbove 90% at temperatures greater than 500^{o}F (260^{o}C). Catalyst A showed a maximum conversion efficiency of 94%. The conversion efficiency of catalyst A began to decrease rapidly below a catalyst temperature of 500^{o}F (260^{o}C). Light-off temperature for CO conversion on catalyst A was 417^{o}F (214^{o}C). Similar performance was noticed on catalyst B, with a maximum conversion efficiency of 95%. The light-off temperature for CO conversion on catalyst B was 410^{o}F (210^{o}C). Catalyst C showed low CO conversion efficiencies. Catalyst C achieved a maximum CO conversion efficiency of 30%. At low catalyst temperatures, catalyst C showed no oxidation of CO. Both catalysts D and E achieved over 95% maximum conversion efficiency. The efficiencies began to decrease at 420^{o}F (215.5^{o}C) for catalyst D and at 400^{o}F (204.5^{o}C) for catalyst E. The conversion efficiency of both the catalysts did not decrease below 50% conversion efficiency at the lowest catalyst temperature achieved. Therefore, the light-off temperatures for catalysts D and E are 370^{o}F (182^{o}C) and below 360^{o}F (182^{o}C) respectively. The light-off temperature indicates the range of temperatures, at which the catalyst can be operated. For a catalyst with lower light-off temperature, it can be operated at a wider temperature range with maximum conversion efficiency.

Environmental Protection Agency have released National Emission Standards for HAPs emission (NESHAP)[13]. According to the standard, the post-catalyst emission of CO has to be equal to (or) less than 7% of pre-catalyst emission. Therefore, it is important to know the catalyst temperature at which the conversion efficiency drops to 93%.

Catalysts A and B were under emission limits for temperature range of 490°F to 800°F according to the NESHAP emission standards. Catalysts D and E were under the limits for a wider temperature range of 400°F (204.5°C) to 800°F (427°C). Catalyst C never achieved the NESHAP emission CO standard.

Figure 21 shows the brake specific CO emission for the oxidation catalysts. The EPA New Source Performance Standards (NSPS) emission standard for CO is 2 g/bhp-hr [2] for engines manufactured since 2010.

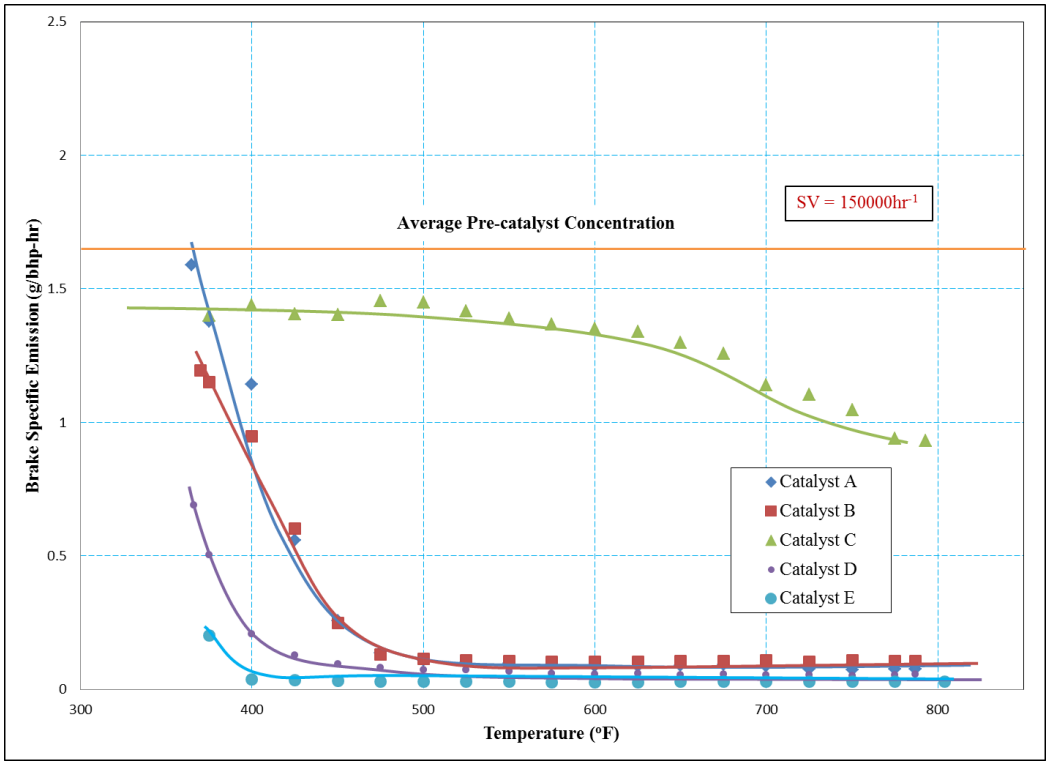

Figure 21: Brake specific CO emission variation with catalyst temperature

Calculated average pre-catalyst CO emission for this engine was 1.65 g/bhp-hr, which is well within the emission standards. Thus, for the Waukesha VGF-18 GL an oxidation catalyst is not necessary to meet the NSPS CO standard.

At low catalyst temperatures, the brake specific CO emission increased rapidly for most oxidation catalysts, but was well within emission limits. Catalyst C had higher brake specific emissions compared to the other oxidation catalysts throughout the tempreature sweep. Catalyst E had very low brake specific CO emission with a maximum brake specific emission of 0.25 g/bhp-hr.

California Code of Regulations released CARB 2006 emission standard for the state of California. The limit for CO emission is 0.034 g/bhp-hr for the state of California[19]. Catalyst A and B were slightly above the CARB 2006 emission standard. Catalyst D met the CARB 2006 emission standard for a catalyst temperature range of 800^{o}F (427^{o}C). to 500^{o}F (260^{o}C). Catalyst E was within the emission limit for catalyst temperatures above 400^{o}F (204.5^{o}C).

3.2 Formaldehyde Emission

Formaldehyde (CH_2O) is a component of HAPs emitted by the engine exhaust. CH_2O emission constitute to over 50% of the total HAPs emission. Figure 22 illustrates the performance of the oxidation catalysts on CH_2O abatement. Average pre-catalyst CH_2O emission was measured at 34 ppm by the FTIR.

Four of the five oxidation catalysts showed over 90% maximum CH_2O conversion efficiency. Catalyst A had a maximum conversion efficiency of 96%. The conversion efficiency of catalyst A decreased rapidly from the maximum catalyst temperature. Light-off temperature for CH_2O conversion on catalyst A was 565^{o}F (296^{o}C). Comparitively, better performance was noticed on catalyst B, with a maximum conversion efficiency of 93%. The light-off temperature for CH_2O conversion on catalyst B was 490^{o}F (254.5^{o}C).

On catalyst B, the CH_2O conversion efficiency began to decrease rapidly at 600°F (315.5°C). Catalyst C showed no CH_2O conversion. Catalyst D and catalyst E showed good activity in CH_2O oxidation, oxidizing over 90% of CH_2O emission. Catalyst E achieved over 95% maximum CH_2O conversion efficiency. Catalyst D had a maximum conversion efficiency of 93%. The light-off tempreature for catalyst E was 490°F (254°C). Catalyst E had a light-off temperature which was below 360°F (182°C).

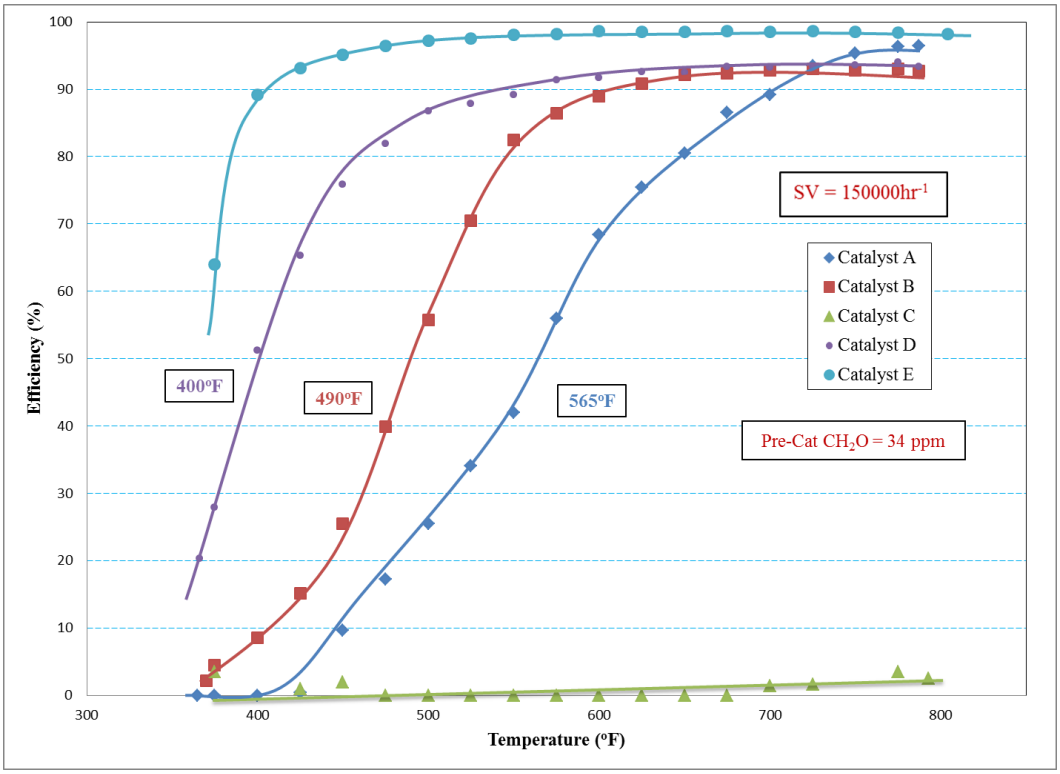

Figure 22: Variation of formaldehyde conversion efficiency with catalyst temperature

The conversion efficiencies decreased at 500°F (260°C) for catalyst D and at 400°F (204.5°C) for catalyst E. The conversion efficiency of catalyst E did not decrease below 50% at the lowest catalyst temperature achieved. Catalyst E achieved a minimum CH_2O

conversion efficiency of 65%. Catalyst E converted over 90% of CH_2O at a catalyst temperature of 400°F (204.5°C).

3.3 Ethylene Emission

Ethylene (C_2H_4) emission is part of the VOC emission from the engine exhaust. VOCs are non-methane, non-ethane, non-formaldehyde hydrocarbons. Figure 23 shows the performance of the oxidation catalysts on C_2H_4 conversion. The average pre-catalyst C_2H_4 emission was measured to be 23 ppm by the FTIR.

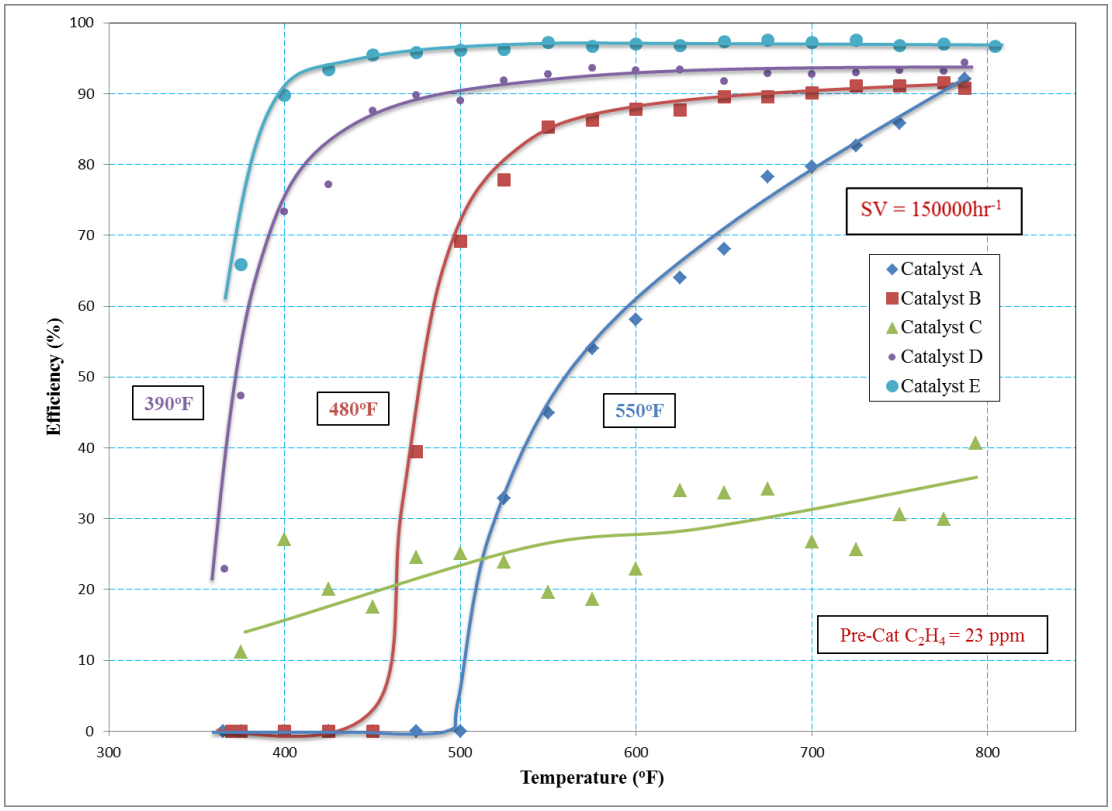

Figure 23: Variation of ethylene conversion efficiency with catalyst temperature

Three oxidation catalysts showed good C_2H_4 conversion efficiencies. Catalyst A had a maximum conversion efficiency of 93%. Light-off temperature for C_2H_4 conversion on

catalyst A was 550°F (288°C). The conversion efficiency of catalyst A began to decrease rapidly with decrease in catalyst temperature. Catalyst B had a maximum conversion efficiency of 92%. The light-off temperature for C_2H_4 conversion on catalyst B was 480°F (249°C). On catalyst B, the C_2H_4 conversion efficiency began to decrease at 550°F (288°C). Catalyst C showed linear trend in C_2H_4 conversion. Catalyst C showed a maximum C_2H_4 conversion efficiency of 40% and decreased to 10% during the temperature sweep. Catalyst D showed over 90% C_2H_4 conversion efficiency for temperatures greater than 500°F (260°C). Light-off temperature for catalyst D was 390°F (199°C), with a maximum conversion efficiency of 95%. The efficiency of catalyst D decreased rapidly at 450°F (232.2°C) catalyst temperature. Catalyst E achieved 98% maximum C_2H_4 conversion efficiency. The light-off tempreature for catalyst E was below 360°F (182.2°C), since it achieved a minimum conversion efficiency of 67%. The efficiency curve shows catalyst E had over 90% conversion efficiency until the catalyst temperature reached 400°F (204.5°C).

Catalyst C data showed scatter of data points due to ethane fluctuations in the fuel. Fuel ethane concentrations affected ethylene concentrations in the exhaust only on catalyst C. This phenomenon was not experienced in the tests on other oxidation catalysts.

3.4 Propylene Emission

Propylene (C_3H_6) emission is also a component of the VOC emission. Figure 24 shows the performance of the oxidation catalysts on C_3H_6 conversion. Pre-catalyst C_3H_6 emission was measured to be 2.3 ppm by the HP 5890 Series II GC.

Most oxidation catalysts showed over 90% C_3H_6 conversion efficiencies. Catalyst A had a maximum conversion efficiency of 100%. The light-off temperature for C_3H_6 conversion on catalyst A was below 360°F (182.2°C). On catalyst A, the C_3H_6 conversion efficiency started to decrease rapidly at 420°F (215.5°C).

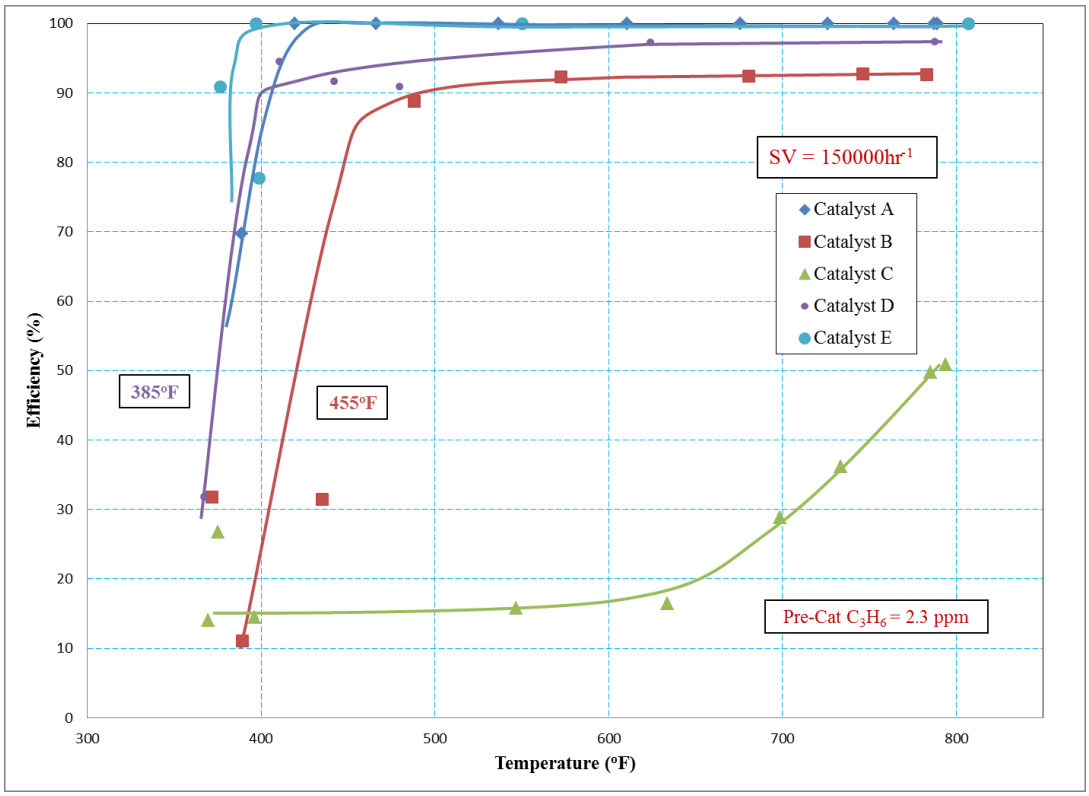

Figure 24: Variation of propylene conversion efficiency with catalyst temperature

Catalyst B had a maximum conversion efficiency of 93%. Light-off temperature for C_3H_6 conversion on catalyst B was 455°F (235°C). The conversion efficiency of catalyst B began to decrease rapidly with decrease in catalyst temperature at 450°F (232.2°C). Catalyst C showed some C_3H_6 conversion. At high exhaust temperatures, catalyst C oxidized 50% of C_3H_6 emission. The conversion efficiency of catalyst C remained constant at 15% after the initial decrease. Catalyst D performed well on C_3H_6 conversion.

Catalyst D had a light-off temperature of 385^{o}F (196^{o}C), with a maximum conversion efficiency of 97%. The efficiency of catalyst D decreased rapidly at 400^{o}F (204.5^{o}C) exhaust temperature. Catalyst E achieved 100% C_3H_6 conversion efficiency almost the entire temperature sweep. The efficiency decreased at temperatures below 400^{o}F (204.5^{o}C). The light-off tempreature for catalyst E was below 360^{o}F (182.2^{o}C), since it achieved a minimum conversion efficiency of 78%.

3.5 Propane Emission

Propane (C_3H_8) emission is the main component of VOC emission from the engine exhaust. VOC emissions are normally characterized by the propane concentrations in the exhaust. Figure 25 show the performance of the oxidation catalysts on C_3H_8 conversion. Pre-catalyst C_3H_8 emission was measured to be 8.0 ppm by the HP 5890 Series II GC.

Low C_3H_8 conversion was noticed on all catalysts. Catalysts A and B showed some amount of C_3H_8 oxidation at high catalyst temperatures. At low catalyst temperatures, scatter of data points were noticed due to the fluctuation in propane concentration in the fuel. Catalysts D and E showed conversion efficiency decrease linearly with catalyst temperature. Catalyst A had a maximum conversion efficiency of 46%, while catalyt B showed a maximum of 63% C_3H_8 conversion. Table 8 shows the activation of hydrocarbons.

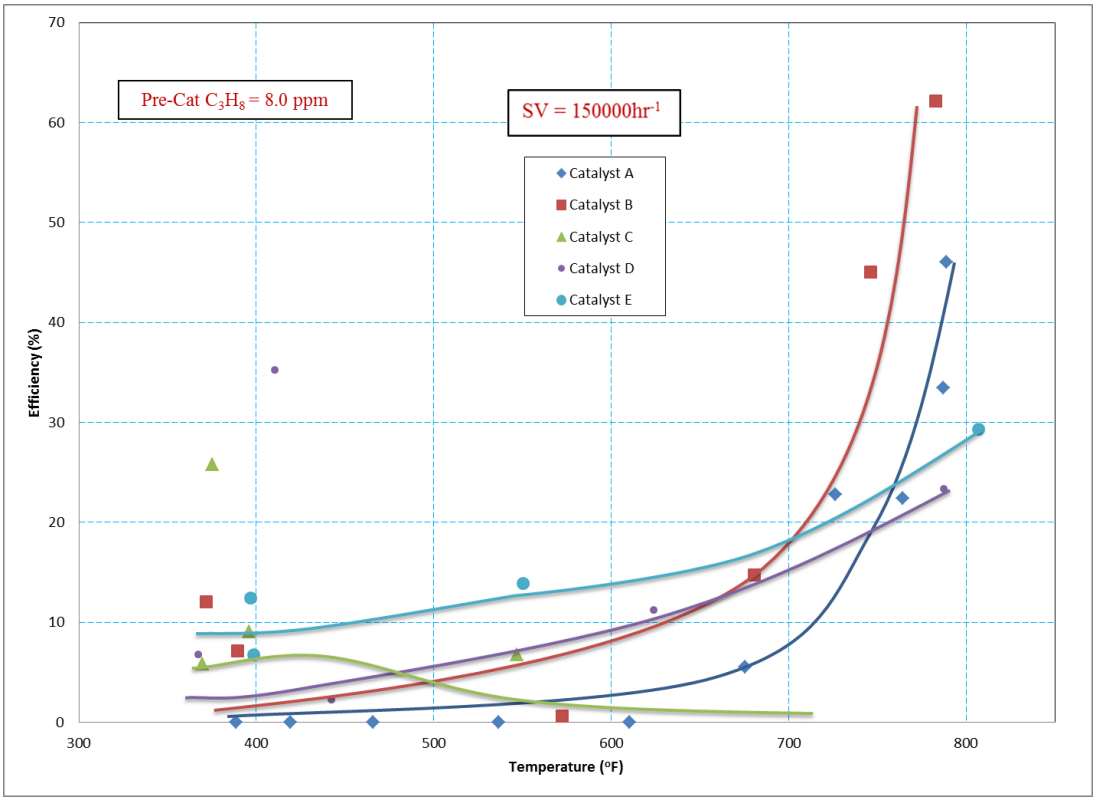

Figure 25: Variation of propane conversion efficiency with catalyst temperature

Table 9: Activation energy for oxidation of hydrocarbons [10]

Hydrocarbon	Pre-exponential term (cm sec^{-1})	Activation energy (kcal mole^{-1})
C_2H_6	$2.8*10^{10}$	27.3
C_3H_8	$1.1*10^{10}$	17.0
C_4H_{10}	$3.3*10^{10}$	17.0
iso-C_4H_{10}	$4.6*10^{10}$	10.2

Catalyst C showed no activity on C_3H_8 conversion. As mentioned earlier, saturated hydrocarbons are difficult to oxidize due to high activation energy. The table also shows

the activation energy decreases with increase in molecular weight. Due to the high activation energy for oxidation of C_3H_8, it is difficult to oxidize.

3.6 VOC Emission

The total VOC emissions was measured by the HP 5890 series II GC. VOCs for the study included species like ethylene, propylene, propane, 1-butene, n-butane, n-pentane and n-hexane. Figure 26 shows the performance of the oxidation catalysts in the conversion of the VOCs. The pre-catalyst concentration of VOCs was measured to be 33 ppm.

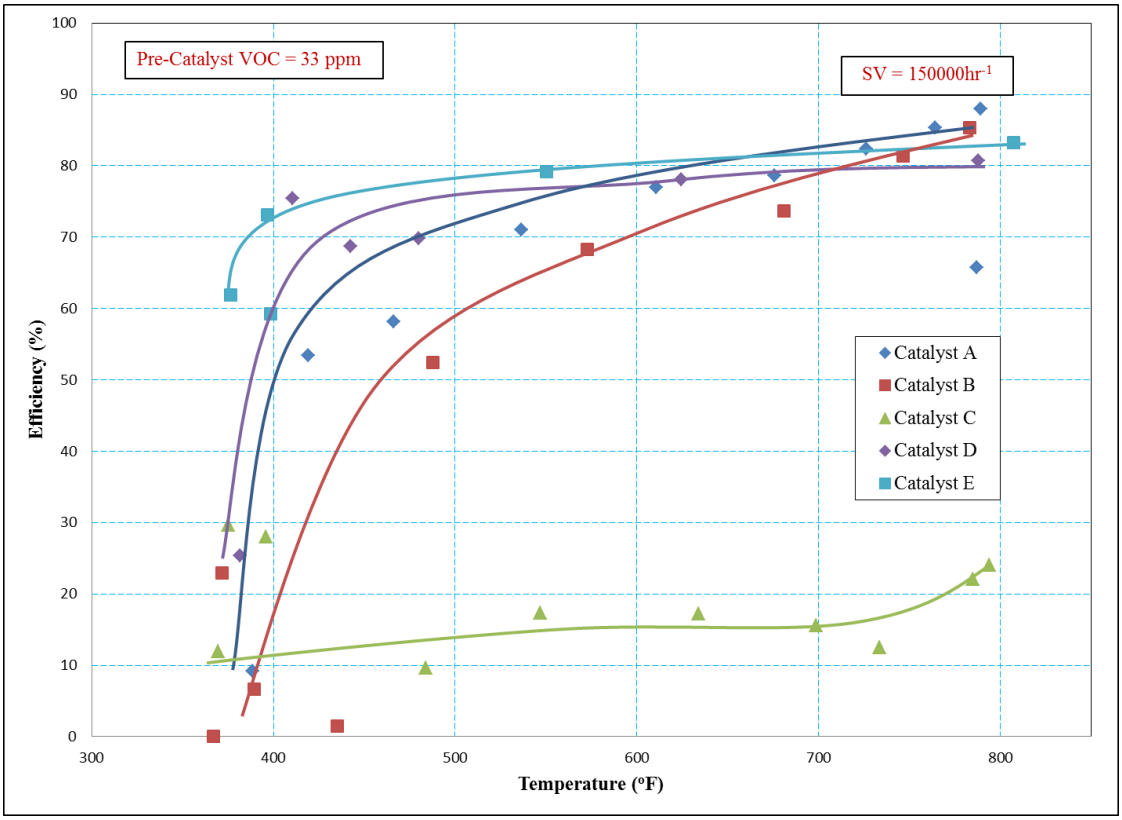

Figure 26: Variation of VOC conversion efficiency with catalyst temperature

Most oxidation catalysts showed good performance on VOC conversion. All the oxidation catalysts showed lower maximum conversion efficiency. This is due to low

conversion efficiencies in C_3H_8 oxidation. Maximum VOC comversion efficiency achieved by most oxidattion catalysts was around 80%. Catalyst A had maximum VOC conversion efficiency of 88%. The efficiency decreased at linearly until the catalyst temperature reached 450^{o}F (232.2^{o}C). Below 450^{o}F (232.2^{o}C), the efficiency decreased at a rapid rate. Catalyst B showed similar trend in VOC conversion with a mazimum conversion efficiency of 86%. Catalyst C showed very little activity on VOC conversion with a maximum conversion efficiency of 22%. The conversion efficiency was steady at around 15% for catalyst C throughout the temperature sweep after the initial decrease in efficiency. Catalysts D and E showed similar trend to catalyst A and B with linear decrease in efficiency. The conversion efficiency decreased linearly with catalyst temperature till 420^{o}F (215.5^{o}C), when the efficiency decreased at a rapid rate.

The heavier hydrocarbons such as butane and higher hydrocarbons were completely oxidized by all the oxidation catalysts. As mentioned in the previous section, the activation energy and autoignition temperature for oxidation decreases with increase in molecular weight. Therefore, all higher hydrocarbons were completely oxidized.

Figure 27 shows the brake specific VOC emission variation with catalyst temperature. Average pre-catalyst brake specific VOC emission was measured to be 0.13 g/bhp-hr. EPA NSPS emission standard states the emission limit for VOCs is 1.0 g/bhp-hr [2]. The pre-catalyst VOC emission was well below the emission limit. The VOC emissions on most oxidation catalysts were well lower than the pre-catalyst emissions. Emission on most catalysts was less than 4% of emission limit at high catalyst temperatures. At 400^{o}F (204.5^{o}C), the VOC emissions began to increase to 10% of the limit at a rapid rate. VOC

emissions from catalyst C was around 0.12 g/bhp-hr during the temperature sweep. No significant conversion of VOCs was noticed on catalyst C.

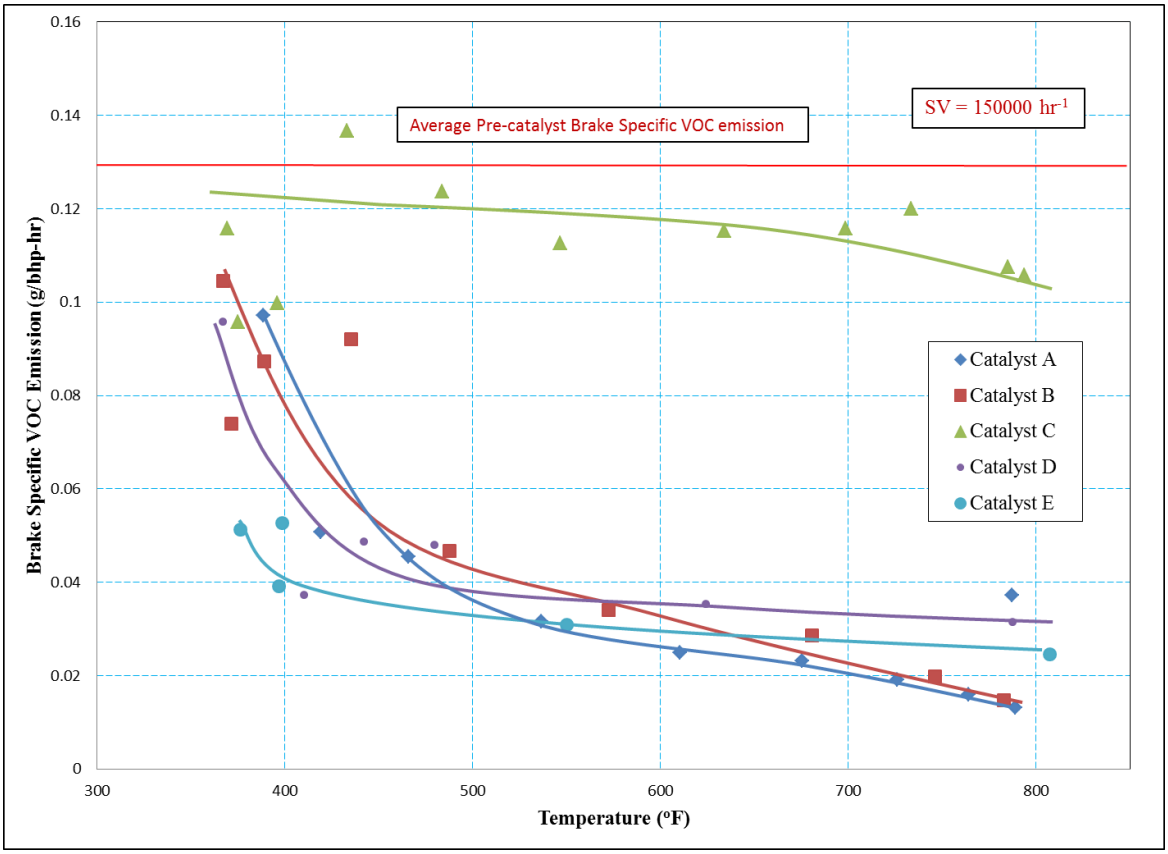

Figure 27: Brake Specific VOC emission variation with catalyst temperature

CARB 2006 emission limit for VOC emission is 0.007 g/bhp-hr [19]. The VOC emission from the oxidation catalysts was more than the CARB 2006 emission standard. The low conversion efficiency of C_3H_8 on all the oxidation catalysts increasing the brake specific VOC emission. Therfore, all the oxidation catalysts did not achieve the CARB 2006 VOC emission standard.

3.6 NO_x Emission

Previous research on oxidation catalysts have shown no or very little activity on NO_x abatement. But, it is important to understand the activity of NO_x in a oxidation catalysts. Figure 28 shows the NO_2/NO_x variation with catalyst temperature. Pre-catalyst NO_2/NO_x was 0.16. Catalyst A, B and D showed similar trends in NO_2/NO_x variation during the temperature sweep. The NO_2/NO_x ratio increased with increase in catalyst temperature. Catalyst D showed increase in NO_2 concentration in NO_x till the catalyst temperature reached 600°F (315.5°C).

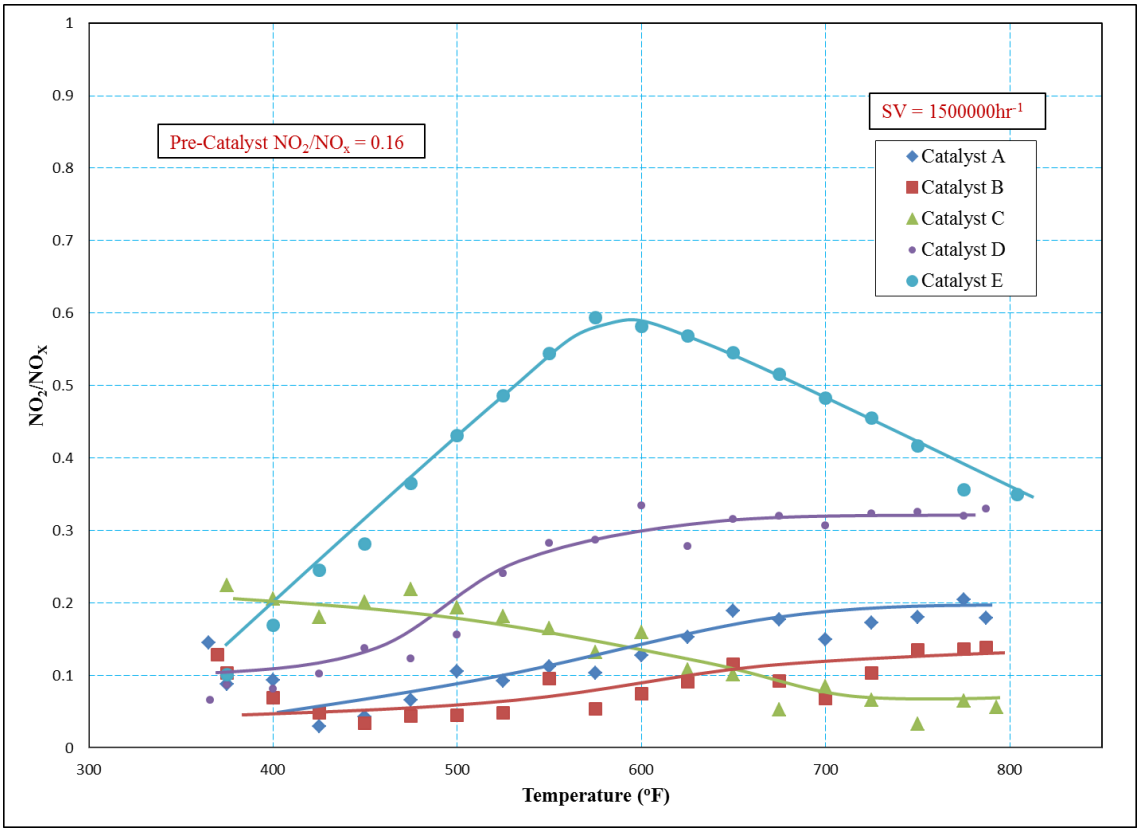

Figure 28: NO_2/NO_x variation with catalyst temperature

Above 600°F (315.5°C), the NO_2/NO_x ratio decreased steadily with catalyst temperature. Catalyst C showed steady increase in NO_2/NO_x ratio with decrease in catalyst temperature.

A thermally favored equlibrium reation shown in equation 3.2 shows NO oxidizes to NO_2. Figure 29 shows the equlibrium calculations for NO_2/NO_x ratio at various temperatures and oxygen percentages.

$$NO + 0.5\ O_2 \leftrightarrow NO_2 \tag{3.2}$$

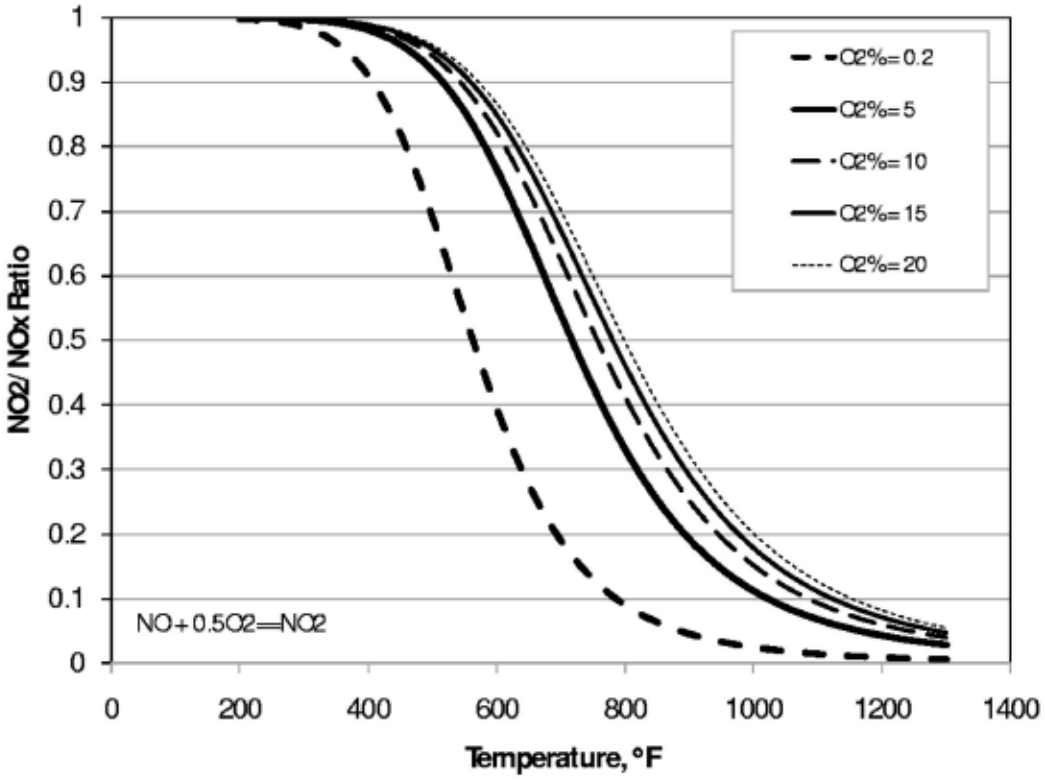

Figure 29: Equilibrium calculations for NO_2/NO_x ratio at various temperatures [15]

The oxidation of NO to NO_2 is favored at low temperatures while the reduction reaction of NO_2 to NO is favored at high temperature [15]. For the oxygen percentage of the study

at 10%, the oxidation of NO to NO_2 is the favored reaction for the temperature range of the study. Thus NO_2 concentration increases with temperature, which was noticed on most catalysts.

Similar trend to catalyst E on NO_x reactions was noticed on the work by Alexander Winkler et. al,[6]. In the work, surface characterization of oxidation catalysts showed change in surface morphology as a possible reason for decrease in NO_2/NO_x ratio. Therefore, apart from chemical equlibrium, surface reactions on an oxidation catalyst surface also affect the NO_x reactions inside the catalysts. No conclusions were reached on the decrease in NO_2 concentration on catalysts C and E due to insufficient data.

4. Space Velocity Variation

Space velocity is the inverse of the residence time of the exhaust gas in the oxidation catalyst in units of hr^{-1}. Reduction in space velocity effectively varies the residence time in the oxidation catalyst. Space velocity can also be correlated to the amount of catalyst material in the oxidation catalyst. Increase in amount of catalyst material increases residence time and reduces space velocity. The focus here is on space velocity, since it is used by catalyst manufacturers and by industry for sizing catalysts for different appliucations. It is necessary to understand the effect of space velocity on the performance of the oxidation catalysts. The catalyst temperature during the variation of space velocity was maintained at a set point of 550^oF (288^oC). The space velocity was varied from maximum to minimum value achievable by the catalyst slipstream with a catalyst envelope volume of approximately 220 in^3.

4.1 CO Emission

Figure 30 shows the performance of oxidation catalysts on CO conversion with varying space velocity. Most catalysts showed over 90% CO conversion efficiency during the space velocity sweep. Increase in CO conversion efficency was noticed on all the oxidation catalysts, with decrease in space velocity. Decrease in space velocity increases the residence time of the exhaust, increasing the probability of emission species oxidizing

inside the catalyst. Catalyst A showed increase in CO conversion efficiency at the initial decrease in space velocity. After the initial increase, the conversion efficiency remained constant during the whole space velocity sweep for catalyst A. Catalyst B showed a similar trend on CO oxidation, relatively lower conversion efficieny than catalyst A. Catalyst C showed no or very little activity on CO oxidation at higher space velocities. The CO conversion efficiency on catalyst C increased at lower space velocities. Catalysts D and E showed over 95% CO conversion efficiency. The conversion efficiencies varied very little for catalyst D and E during the space velocity sweep.

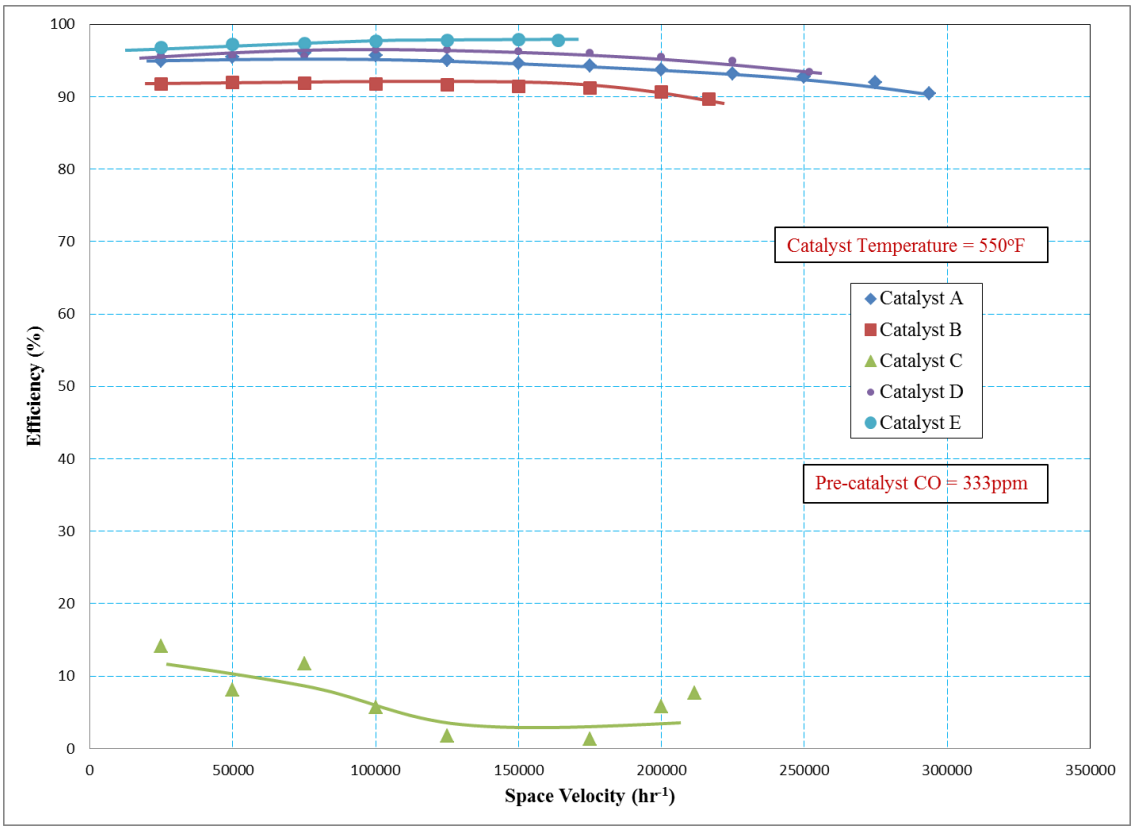

Figure 30: Variation of CO conversion efficiency with space velocity

The maximum value on space velocity achieved on each oxidation catalyst was different. Space velocity is calculated using the formula shown in Equation 4.1.

$$\text{Space Velocity} = \frac{\text{Standard exhaust flow rate}}{\text{Envelope volume of the catalyst}} \quad (4.1)$$

The usable envelope volume of each catalyst module was different due to differences in frame design. Therefore, the maximum space velocity achieved by each catalyst module was different.

4.2 Formaldehyde Emission

Figure 31 shows the variation of CH_2O conversion efficiency with space velocity. Significant variation in the performance of oxidation catalysts on CH_2O conversion was observed in the space velocity sweep.

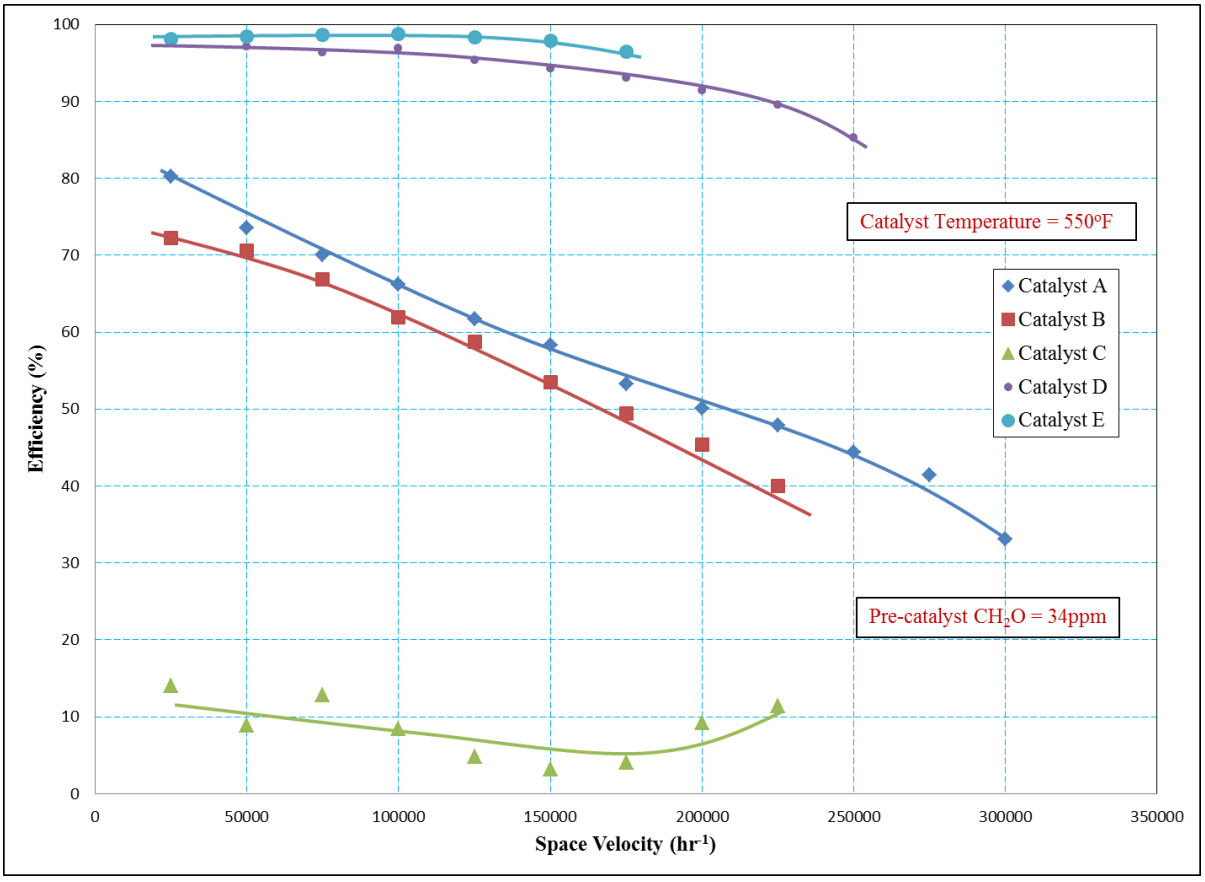

Figure 31: Variation of formaldehyde conversion efficiency with space velocity

Catalyst A showed a linear increase in CH_2O conversion efficiency with decrease in space velocity. The conversion efficiency increased from 33% to 80% during the space velocity sweep for catalyst A. CH_2O conversion efficiency for catalyst B showed a similar trend to catalyst A, increasing linearly with decrease in space velocity. CH_2O conversion efficiency on catalyst B increased by 30% during the space velocity sweep. Catalyst C showed increase in oxidation of CH_2O at lower space velocities. Catalyst D showed over 90% conversion of CH_2O during the space velocity sweep. The conversion efficiency increased during the space velocity sweep, until it reached a maximum of 98% at the lowest catalyst space velocity. Catalyst E showed near 100% CH_2O conversion at low space velocities. The CH_2O conversion efficiency on catalyst E showed increase at higher space velocities, but remained constant at lower space velocities.

4.3 Ethylene Emission

For this engine class, ethylene (C_2H_4) emission typically makes up the largest percentage (68%) of VOC emission. Figure 32 shows the variation of C_2H_4 conversion efficiency with space velocity.

Most oxidation catalysts showed near 100% C_2H_4 conversion efficiency during the space velocity sweep. Catalyst A oxidized all the C_2H_4 during the space velocity sweep. Catalyst B showed 98% C_2H_4 conversion efficiency throughout the space velocity sweep. Some oxidation of C_2H_4 was measured on catalyst C. At higher space velocities, catalyst C oxidized around 25% of C_2H_4 in the exhaust. Catalyst C showed a increase in conversion efficiency at the initial decrease in space velocity and remained constant for the remaining space velocity sweep.

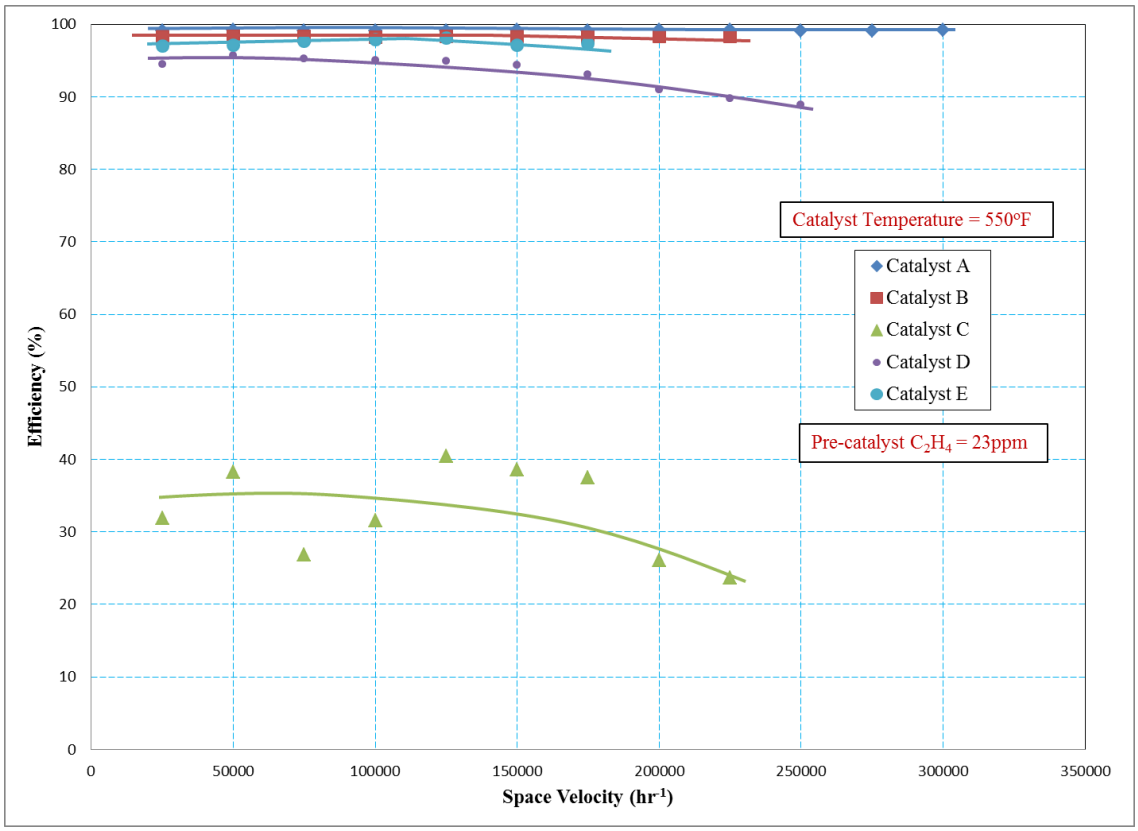

Figure 32: Variation of ethylene conversion efficiency with space velocity

Catalyst D and E showed over 90% C_2H_4 conversion efficiency during the space velocity sweep. Catalyst D showed increase in C_2H_4 conversion efficiency with decrease in space velocity. C_2H_4 conversion efficiency on catalyst E remained constant at 97% during the space velocity sweep.

4.4 Propylene Emission

Propylene (C_3H_6) emission is also a component of VOC emission. C_3H_6 emission constitutes about 7% of VOC emission. Figure 33 shows the variation of C_3H_6 conversion efficiency with space velocity.

Most oxidation catalysts showed near 100% C_3H_6 conversion efficiency during the space velocity sweep. The C_3H_6 conversion efficiency on catalyst A increased with decrease in space velocity until the conversion efficiency reached 100%. At lower space velocities Catalyst A oxidized all the C_3H_6 emission. Catalyst B showed over 98% C_3H_6 conversion efficiency throughout the space velocity sweep. Intial decrease in space velocity showed a increase in conversion efficiency for catalyst B. After the initial increase, no increase of conversion efficiency was noticed on catalyst B. Some oxidation of C_3H_6 was noticed on catalyst C at lower space velocities. No C_3H_6 conversion was noticed on catalyst C at higher space velocities.

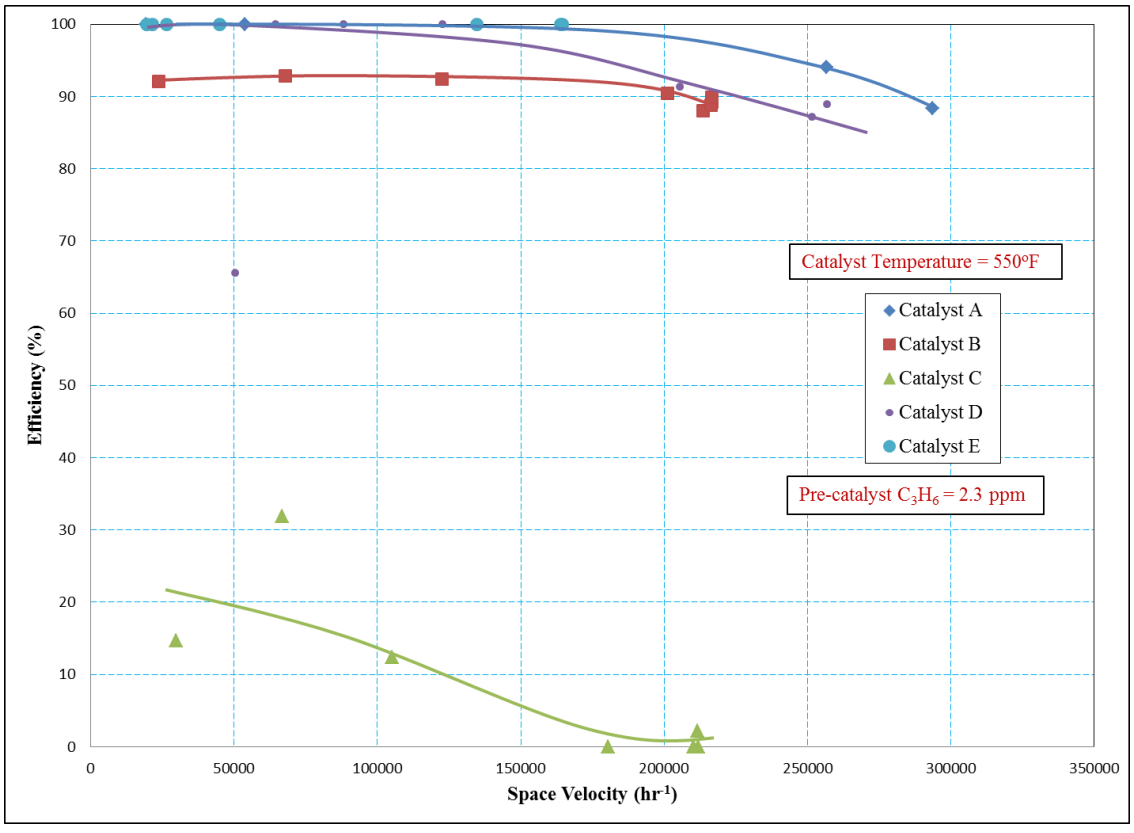

Figure 33: Variation of propylene conversion efficiency with space velocity

Catalyst D showed over 90% C_3H_6 conversion efficiency. Catalyst D showed increase in C_3H_6 conversion efficiency with decrease in space velocity. At 50000 hr^{-1} space velocity, catalyst D showed low C_3H_6 conversion efficiency of 67% with a emission concentration of 0.6 ppm. The fluctuations in propane concentration caused the variation in C_3H_6 emission. Catalyst E showed 100% C_3H_6 conversion efficiency during the space velocity sweep.

4.5 Propane Emission

Propane (C_3H_8) emission is an important constituent of VOC emissions because it is usually present in significant quantities and is difficult to oxidize. Average pre-catalyst C_3H_8 concentration was measured to be 8 ppm and constituted 24% of VOC emission. In the previous chapter, it was shown that the oxidation catalysts showed very little or no activity on C_3H_8 conversion. Figure 34 shows the variation of C_3H_8 conversion efficiency with space velocity.

A linear trend in C_3H_8 conversion efficiency was noticed on most oxidation catalysts with decrease in space velocity. Catalyst A showed no change in C_3H_8 conversion efficiency with change in space velocity. Catalyst B showed increase in C_3H_8 conversion efficiency with decrease in space velocity. Catalyst C showed decrease in C_3H_8 conversion with decrease in space velocity.

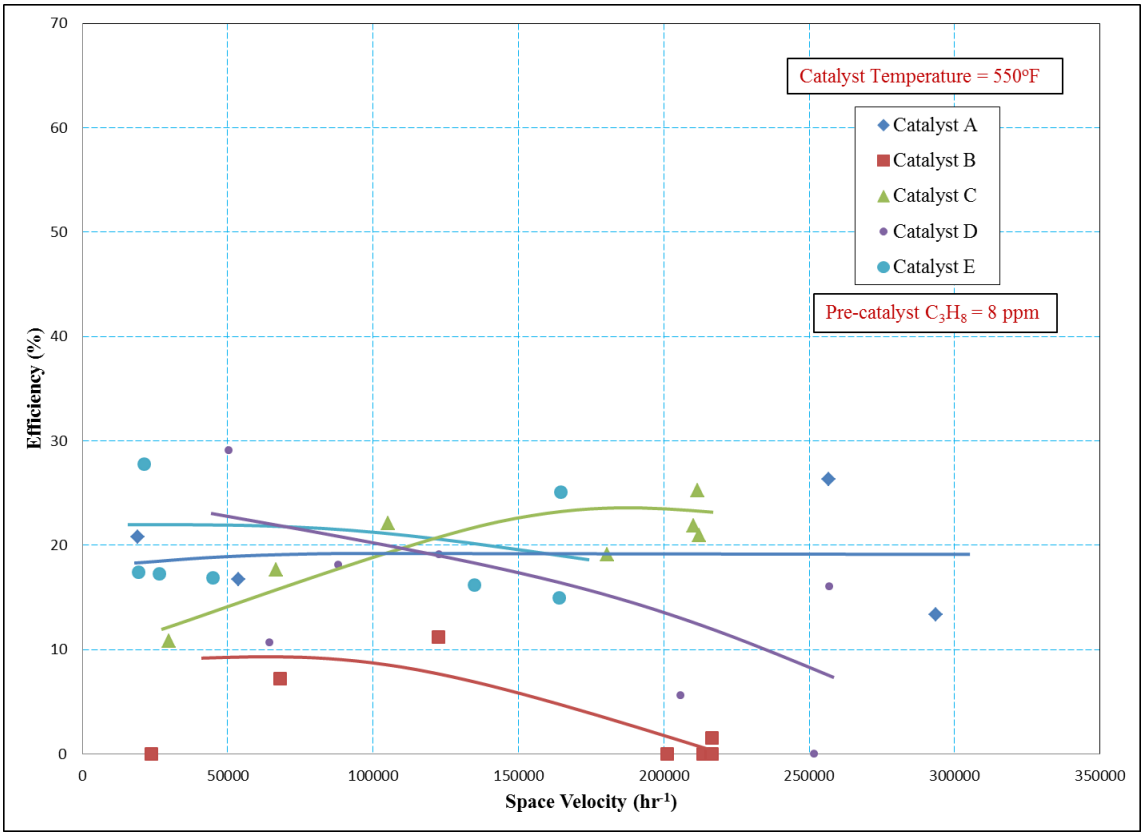

Figure 34: Variation of propane conversion efficiency with space velocity

This trend was due to the fluctuations in pre-catalyst C_3H_8 concentrations. Catalysts D and E followed the trend of increasing conversion efficiency with decreasing space velocity.

4.6 VOC Emission

VOC emission included all non-methane and non-ethane hydrocarbons. As discussed in the previous section, very little conversion of C_3H_8 was seen on all catalysts. C_3H_8 constitutes about 20% of VOC emission from the exhaust. C_3H_8 reduction efficiency is relatively low, therefore the maximum conversion efficiency of VOCs. Figure 35 shows

the variation of VOC conversion efficiency with space velocity for the oxidation catalysts.

Catalyst A showed an increase in VOC conversion efficiency with decreasing in space velocity. Similar trends were observed on catalysts B, D and E. Conversion efficiency on catalyst B was lower than catalyst A. VOC conversion efficiency on catalyst D increased at higher space velocities, but remained constant at lower space velocities. Catalyst C showed very little VOC conversion.

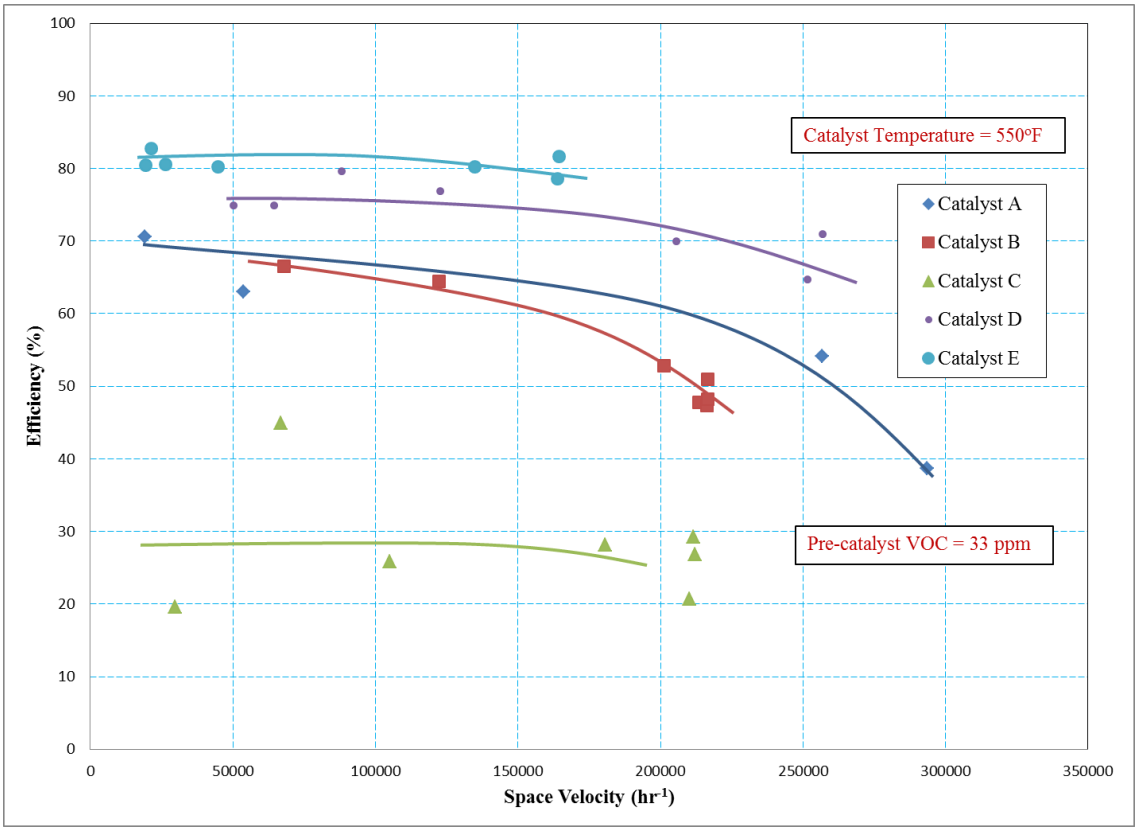

Figure 35: Variation of VOC conversion efficiency with space velocity

The VOC conversion efficiency for catalyst E remained around 80%. Catalyst C showed very little change on VOC conversion efficiency during the space velocity sweep. VOCs

can react with NO_2 to form CO_2, NO and water. VOCs also react with O_2 to form CO_2 and water.The global reaction for ethylene with NO_2 is shown in Equation 4.2.

$$C_2H_4 + 6NO_2 \rightarrow 2CO_2 + 2H_2O + 6NO \quad (4.2)$$

Similar to Equation 4.2, all other VOC species react with NO_2 to form CO_2, NO and water. Ethylene has a VOC reactive index of 2.21, while the reactive index for propane is 0.25 [17]. Compounds with higher reactivity index readily react with NO_2 and/or O_2.

4.7 NO_x Emission

Variation of NO_x composition across the oxidation catalyst is important to understand. NO2 is approximately 5 times toxic as NO and it impacts visibility since it is a colored gas [20]. Figure 36 shows the variation of NO_2/NO_x ratio with space velocity.

The equilibrium reaction between oxidation of NO and reduction of NO_2 is temperature dependant. The catalyst temperature for the space velocity sweep was maintained at 550^{o}F (288^{o}C). At this catalyst temperature, the equilibrium reaction favors oxidation of NO to NO_2. Based on the mechanism, NO_2/NO_x ratio increases with decreasing space velocity. Decrease in space velocity increases the residence time inside a catalyst, providing more time for oxidation of NO to NO_2. This trend of increasing NO_2 concentration was measured on most oxidation catalysts. Catalyst A showed a increase in NO_2 concentration at lower space velocity, remaining constant at higher space velocities. Very little variation of NO_2 concentration was noticed on catalyst B.

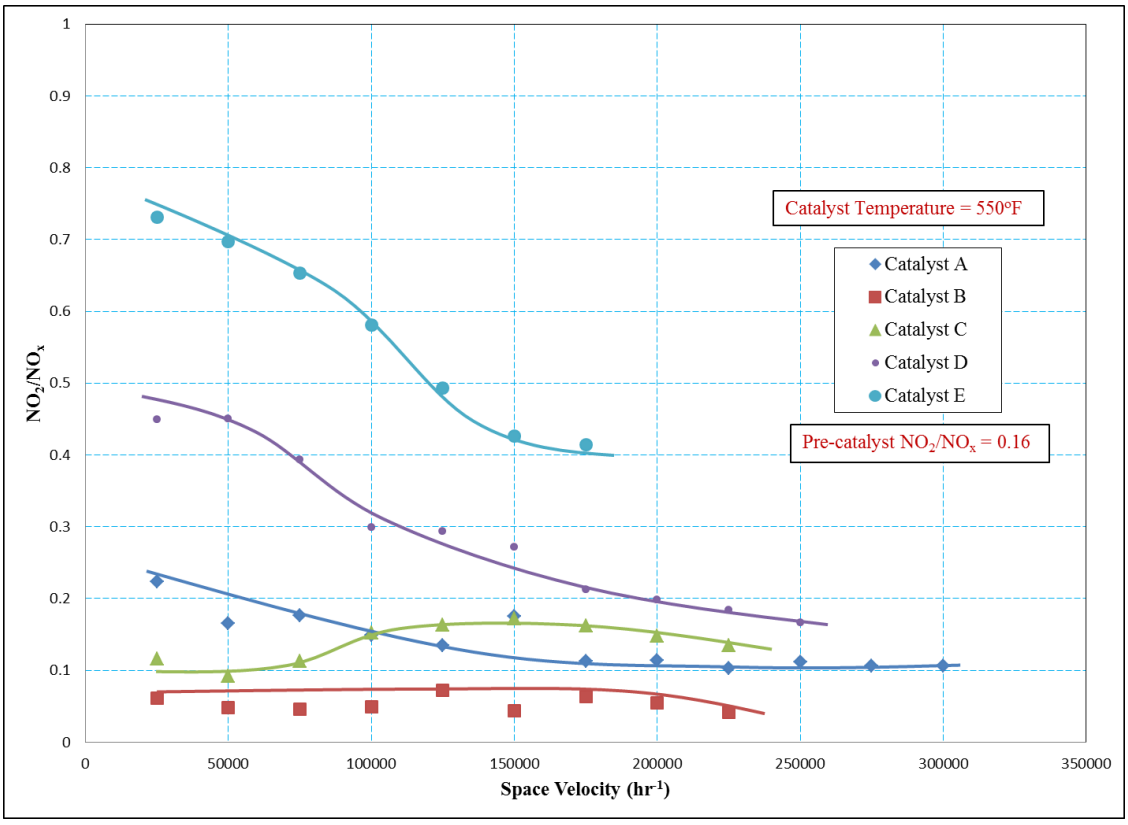

Figure 36: Variation of NO_2/NO_x ratio with space velocity

Catalyst C and D showed similar trends in NO_2 concentration, increasing with decrease in space velocity. Catalyst E showed decrease in NO_2 concentration at lower space velocity. As mentioned in the previous section, NO_x reaction mechanisms are dependant on surface reactions. The catalyst temperature was maintained at a setpoint value of 550°F, the rate of increase of NO_2/NO_x ratio is different on most oxidation catalysts. Therfore, NO_x reaction mechanism inside an oxidation catalyst is dependant on both thermally favored chemical equilibrium reactions and kinetically dependant surface reaction mechanisms. The trend of decrease in NO_2 concentration with decreasing space velocity on catalyst C is inconclusive due to insuffient data for analysis.

4.8 Friction Factor Correlation

The oxidation catalysts used in the study varied in cell density from 200 cells/in^2 (31 cells/cm^2) to 600 cells/in^2 (93 cells/cm^2). The test results showed no or very little effect of cell density on the performance of the oxidation catalysts. The cell density of the oxidation catalysts affected the pressure drop across the catalysts. The pressure drop across the catalyst was directly proportional to cell density. Oxidation catalysts with higher cell density caused higher pressure drop across the catalyst due to increased obstruction to the flow.

Figure 37 shows the variation in differential pressure across the catalyst with space velocity for the oxidation catalysts. The differential pressure for catalyst A varied from 1.2 to 5.1 inches of water (0.002 to 0.12 bar) with a cell density of 600 cells/in^2 (93 cells/cm^2). Catalyst B had a differential pressure ranged from 0.95 to 2.5 inches of water (0.0023 to 0.0062 bar). Catalyst B had a cell density of 300 cells/in^2 (46 cells/cm^2). Catalyst C had a cell density of 300 cells/in^2 (46 cells/cm^2) and showed the differential pressure range from 0.8 to 3.2 inches of water (0.0019 to 0.0079 bar). Catalyst D had the lowest cell density of 200 cells/in^2 (31 cells/cm^2). The differential pressure for catalyst D ranged from 0.5 to 2.4 inches of water (0.0012 to 0.0059 bar). The differntial pressure for catalyst E ranged from 0.5 to 2.5 inches of water (0.0012 to 0.0062 bar) with a cell density of 300 cells/in^2 (46 cells/cm^2). The differential pressure for most catalysts varied linearly with space velocity.

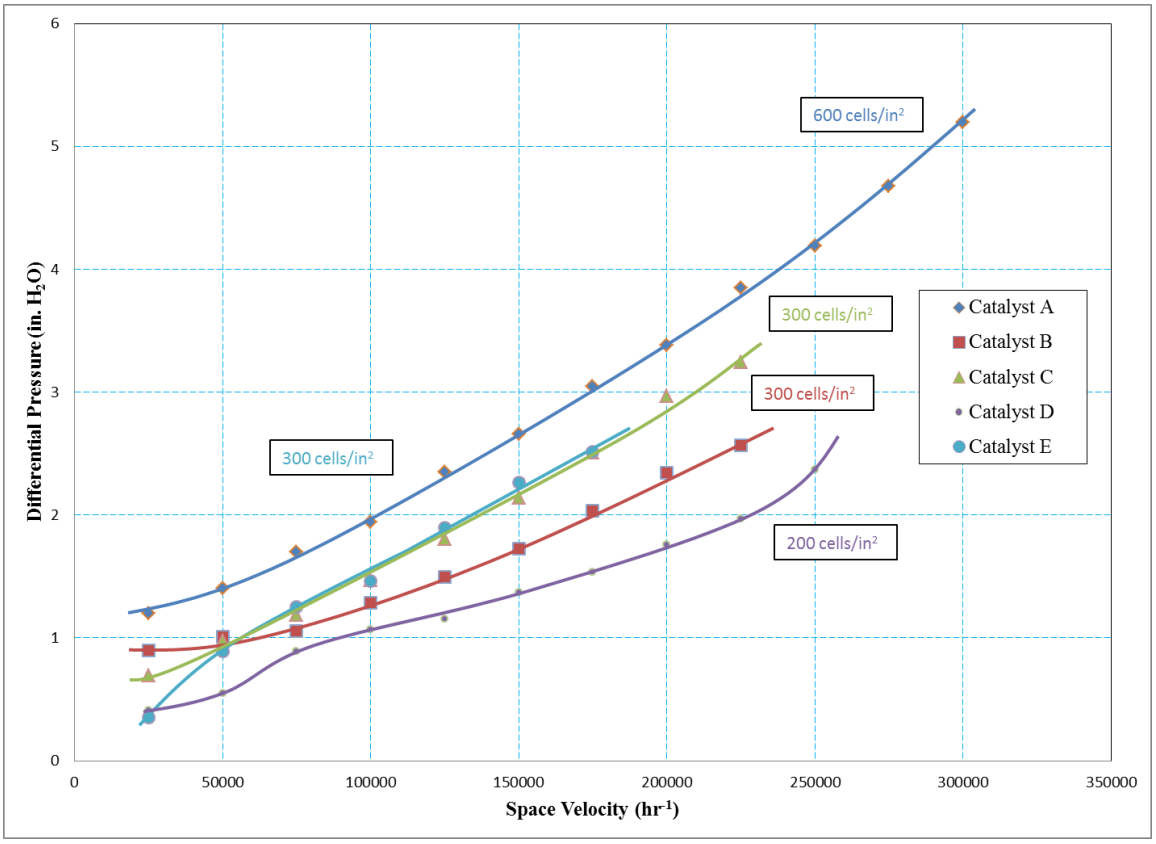

Figure 37: Variation of differential pressure with space velocity

The differential pressure for catalyst B was much lower than other catalysts with same cell density. The catalyst substrate for catalyst B is designed to reduce pressure drop and increase turbulance to the flow inside the catalyst module.

The pressure drop across the catalyst was used to calculate friction factor for the flow through the catalyst. Figure 38 shows the variation of friction factor with Reynolds number.

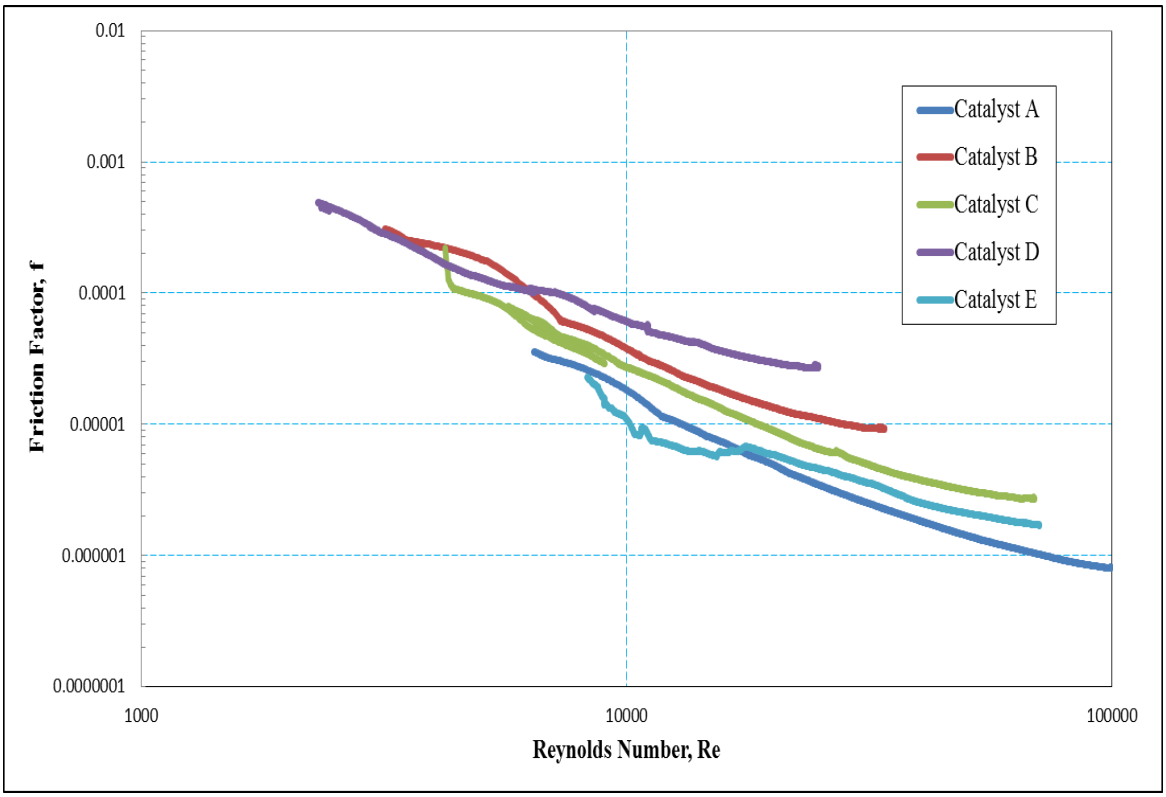

Figure 38: Variation of friction factor with Reynolds number

Equation 4.3 was used to calculate the friction factor for each oxidation catalyst.

$$\text{Friction factor, f} = \frac{\text{h}}{\left(\frac{\text{l}}{\text{d}}\right)*\left(\frac{\nu^2}{2g}\right)} \tag{4.3}$$

In the equation 4.3, h is the pressure head or pressure drop across the catalyst, l is the length of the catalyst module, d is the diameter of each cell, ν is the velocity of the flow through the catalyst and g is the acceleration due to gravity. The velocity, ν is calculated from the space velocity and catalyst volume.

Equation 4.4 shows the formula used for the calculation of Reynolds number.

$$\text{Reynolds Number, } Re = \frac{Vd}{\nu} \tag{4.4}$$

V in the equation 4.4 denotes the actual volume flowrate through the catalyst module.

This analysis was developed to understand the effect of cell density on the performance of the oxidation catalyst. Oxidation catalysts with lower cell density showed higer range of friction factor. The range of friction factor decreased with cell density.

Results in the current chapter showed, cell density had no or very little effect on reduction of oxidation catalysts. Catalyst A had the highest cell density of 600 cells/in^2, performed similar to other oxidation catalysts with lower cell densities during the space velocity sweep.

5. Conclusion

Emission from lean burn natural gas engines used for power generation and gas compression are major contributors to air pollution. Two-way catalysts or oxidation catalysts are the common after-treatment system used on lean burn natural gas engines to reduce emissions of products of partial combustion (CO, CH_2O and VOCs). The performance of the oxidation catalysts is dependent on operating parameters like catalyst temperature and space velocity. The study was done to understand the effect of these operating parameters on the performance of oxidation catalysts and to evaluate how significant differences are between catalyst vendors.

For the study, a part of exhaust from a Waukesha VGF-18 GL lean burn natural gas engine was used. The catalyst slipstream used in the study allowed control over the catalyst operating parameters without affecting engine operating parameters. Emission analyzers, 5-gas, FTIR and HP 5890 Series II GC, were used for the measurement of emission species. The oxidation catalysts were degreened at 1200^{o}F (650^{o}C) for 24 hours. The performance of oxidation catalysts was analyzed for varying catalyst temperature and space velocity.

Catalyst Temperature

Most oxidation catalysts showed over 90% CO conversion efficiencies with light-off temperatures ranging from 417^{o}F (214^{o}C) to less than 360^{o}F (182^{o}C). Most oxidation catalysts showed over 90% maximum CO conversion. CO conversion efficiencies on catalyst D and E did not decrease below 50%. Good CH_2O conversion efficiencies were noticed on most of the oxidation catalysts. The light-off temperature for CH_2O ranged

from 565°F (296°C) to below 360°F (182°C). Over 90% maximum C_2H_4 conversion efficiencies were noticed with light-off temperature ranging from 550°F (288°C) to below 360°F (182°C). High conversion efficiencies were noticed on C_3H_6 with some oxidation catalysts showing 100% conversion efficiency at high catalyst temperatures. No or very little C_3H_8 conversion was noticed on the oxidation catalysts. At high catalyst temperatures, the oxidation catalysts showed an increase in C_3H_8 conversion efficiency. Saturated hydrocarbons such as propane are difficult to oxidize in a oxidation catalyst due to high activation energy and autoignition temperature. All oxidation catalysts oxidized VOCs, with maximum conversion efficiency at 80%. VOC reduction was limited by propane emission. Therefore, development of new catalyst formulation is needed to improve conversion efficiency of VOCs. Oxidation of NO to NO_2 was noticed on most oxidation catalysts, which is favored based on chemical equlibrium. Table 5 shows the summary of results from the study.

Space Velocity

Variation in space velocity showed very little effect on the conversion efficiencies. Most species showed over 90% conversion efficiency on emission species. The conversion efficiency of the species varied very little with change in space velocity for most emission species. Over 90% CO conversion efficiency was observed on most most oxidation catalysts. Less than 3% change in CO conversion efficiency was observed during space velocity sweep. CH_2O reduction efficiency was constant for most oxidation catalysts. Some oxidation catalysts showed increase in CH_2O conversion efficiency with decrease in space velocity. 100% C_2H_4 conversion was noticed on most catalysts during the space velocity sweep. All the oxidation catalysts showed increase in C_3H_6 conversion

efficiency with decrease in space velocity, until the conversion efficiency reached 100%. Very little oxidation of C_3H_8 was observed on any of the oxidation catalysts with decreasing space velocity. 80% VOC reduction efficiency was observed on most catalysts during the space velocity sweep. No change on performance of the oxidation catalysts was noticed for varying space velocities after conversion efficiencies reached 90%. Therefore, adding more catalyst volume may not increase reduction efficiency of emission species. The varying cell density showed very little effect on performance of the oxidation catalysts. The friction factor correlation showed the friction factor is inversely proportional to cell density.

The reduction efficiencies for emission species tested, varied substantially among the oxidation catalysts provided by different vendors.

Table 10: Summary of results from the study

	Light Off Temperature					Maximum Conversion Efficiency					Maximum Pressure Drop (in. H_2O)	Average Cell Density (cells/in^2)
	CO	CH_2O	C_2H_4	C_3H_6	C_3H_8	CO	CH_2O	C_2H_4	C_3H_6	C_3H_8		
Catalyst A	410°F	565°F	550°F	<360°F		95%	96%	93%	100%	54%	5.2	600
Catalyst B	417°F	490°F	480°F	455°F		92%	93%	92%	93%	62%	2.56	300
Catalyst C						31%	3%	40%	51%	25%	3.25	300
Catalyst D	<360°F	400°F	390°F	385°F		96%	93%	95%	97%	35%	2.4	200
Catalyst E	<360°F	<360°F	<360°F	<360°F		98%	98%	98%	100%	30%	2.53	300

References

[1] John B. Heywood, "Internal Combustion Engines Fundamentals", Textbook, 1988

[2] Environmental Protection Agency, "Standards of performance for stationary spark ignition internal combustion engines and national emission standards for hazardous air pollutants for reciprocating internal combustion engines; Final Rule", Federal Register, Vol. 73, No. 13, 2008

[3] Shazam Williams et. al., "Oxidation Catalysts for Natural Gas Engine operating under HCCI or SI conditions", SAE International Journal of Fuels Lubrication, 2008-01-0807

[4] Jordan K. Lampert et. al., "Palladium catalyst performance for methane emissions abatement from lean burn natural gas vehicles", Applied Catalysis B: Environmental 14 (1997) 211-223

[5] Robert L. McCormick et. al., "Rapid Deactivation of Lean burn Natural Gas Engine Exhaust Oxidation Catalyst", Sensors And Actuators, 1996, Vol. 1206, 63-77

[6] Alexander Winkler et. al., "The influence of chemical and thermal aging on the catalytic activity of a monolithic diesel oxidation catalyst", Applied Catalysis B: Environmental 93 (2009) 177–184

[7] Hiromichi Yamamoto and Hiroshi Uchida, "Oxidation of methane over Pt and Pd supported on alumina in lean-burn natural-gas engine exhaust", Catalysis Today, 45 (1998) 147-151

[8] Deborah L. Mowery et. al., "Deactivation of $PdO–Al_2O_3$ oxidation catalyst in lean-burn natural gas engine exhaust: aged catalyst characterization and studies of poisoning by H_2O and SO_2", Applied Catalysis B: Environmental 21 (1999) 157–169

[9] Shin'ichi Matsumoto, "Catalytic Reduction of Nitrogen Oxides in Automotive Exhaust Containing Excess Oxygen by NOx Storage-Reduction Catalyst", CATTECH, Volume 4, Number 2, 102-109

[10] Leon Hiam et. al., "Catalytic oxidation of hydrocarbons on platinum", Journal of Catalysis, Volume 10, Issue 3, 1968, 272-276

[11] Joshua C. Schmitt, "Selective catalytic reduction: testing, numeric modeling and control strategies", Master's Thesis, Colorado State University, Spring 2010

[12] Kristopher Quillen, "Engine fiction reduction measurements and particulate measurements of a lean burn 4-stroke natural gas internal combustion engine", Master's Thesis, Colorado State University, Spring 2007

[13] Environmental Protection Agency, "National emission standards for hazardous air pollutants for reciprocating internal combustion engines", Federal Register, Vol. 76, No. 46, 2011

[14] Thormählen, et. al., "Low-Temperature CO Oxidation over Platinum and Cobalt Oxide Catalysts", Journal of Catalysis, Volume 188, Issue 2, 1999, 300-310

[15] Daniel Olsen et. al., "Impact of oxidation catalysts on exhaust NO2/NOx ratio from lean burn natural gas engine", Journal of Air and Waste Management Association, 60 (2010) 867-874

[16] Coward H.F. and Jones G.W., “Limits of Flammability of Gases and Vapors”, Bulletin 503, U.S. Department of the Interior, Bureau of Mines, 1952

[17] Carter W. P. L, “SAPRC Atmospheric chemical mechanisms and VOC reactivity scales”, Air pollution research center and college of engineering center for environmental research and technology, University of California, Riverside, www.cert.ucr.edu/~cater/SAPRC

[18] Frank White, “Fluid mechanics”, Textbook, Seventh edition, 2009

[19] California Code of Regulations, “Amendments to the distributed generation certification regulation”, Article 3, Division 3 of title 17, 2003

[20] J. A. Last et. al., “Ozone, NO and NO2: oxidant air pollutants and more”, Environmental Health Perspectives, 102 (Suppl 10), 1994, 179-184

[21] HP 5890 Series II and HP 5890 Series II Plus operating manual